

CHAPTER 2

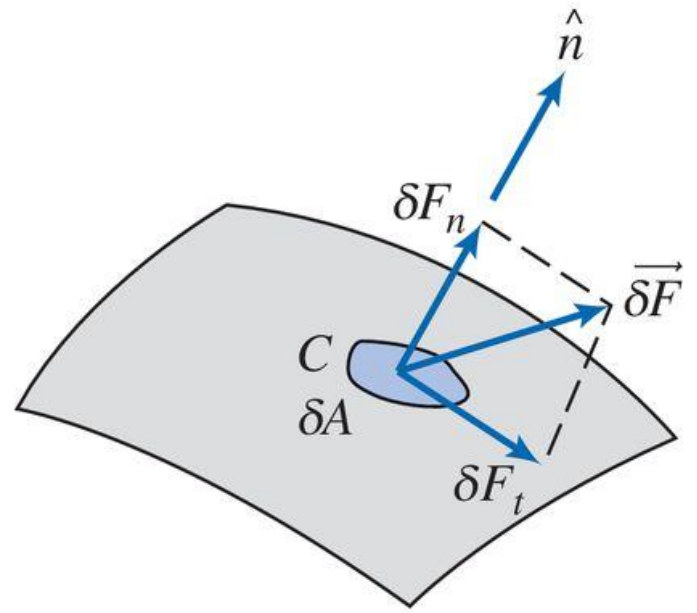
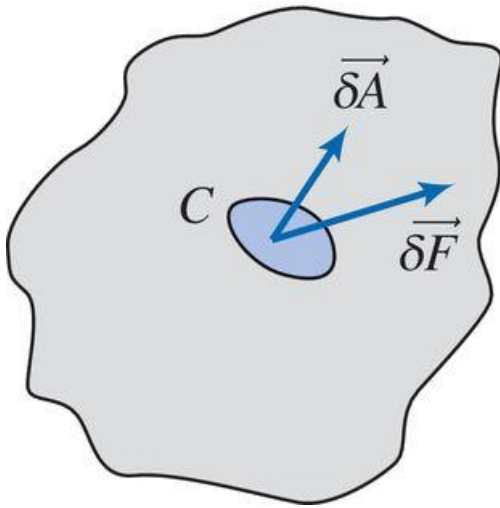


Figure 2.6

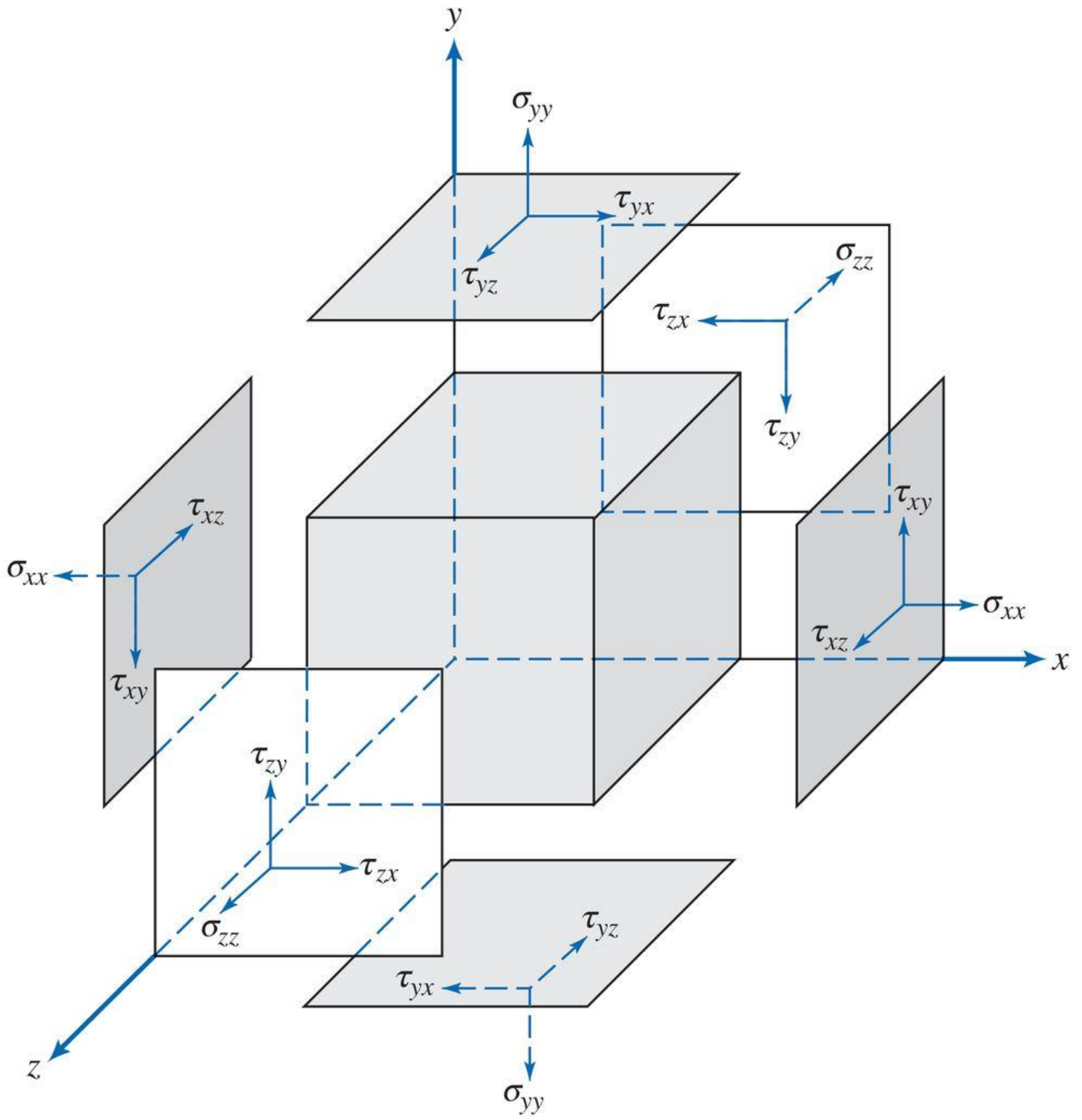
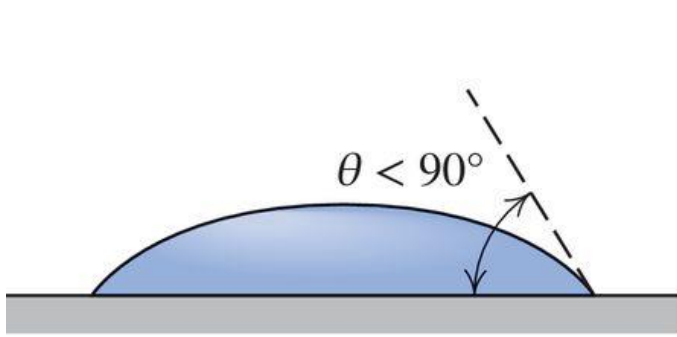
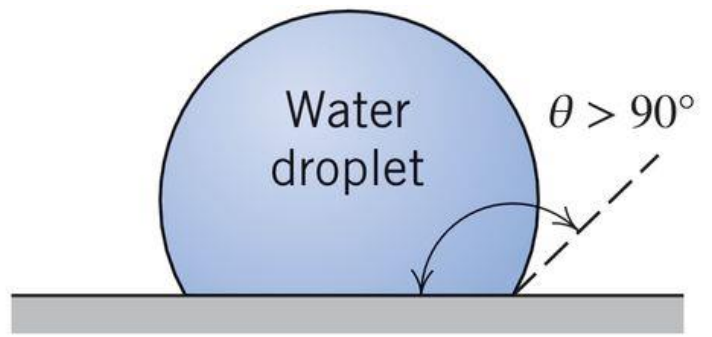


Figure 2.8

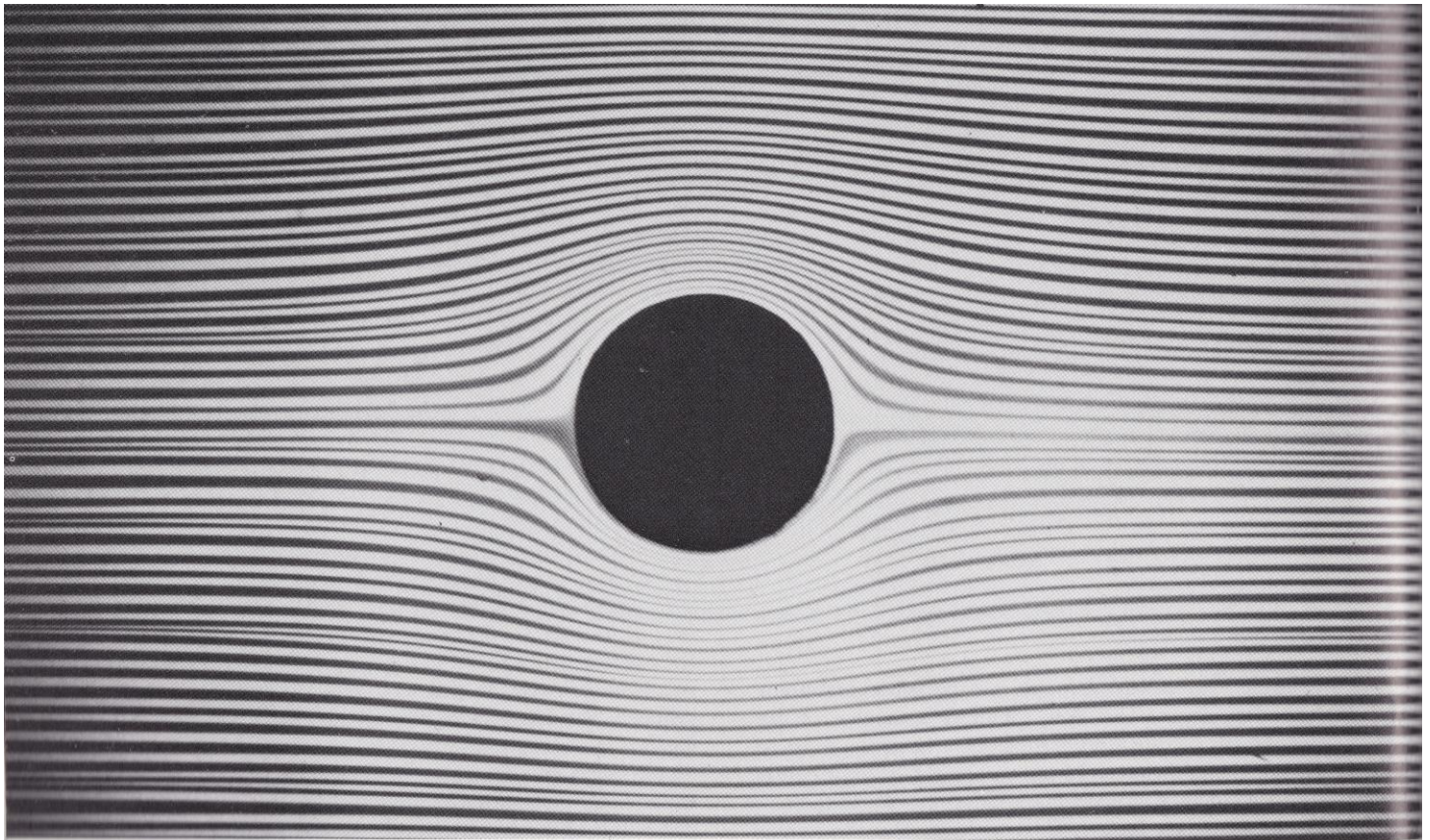


(a) A “wetted” surface



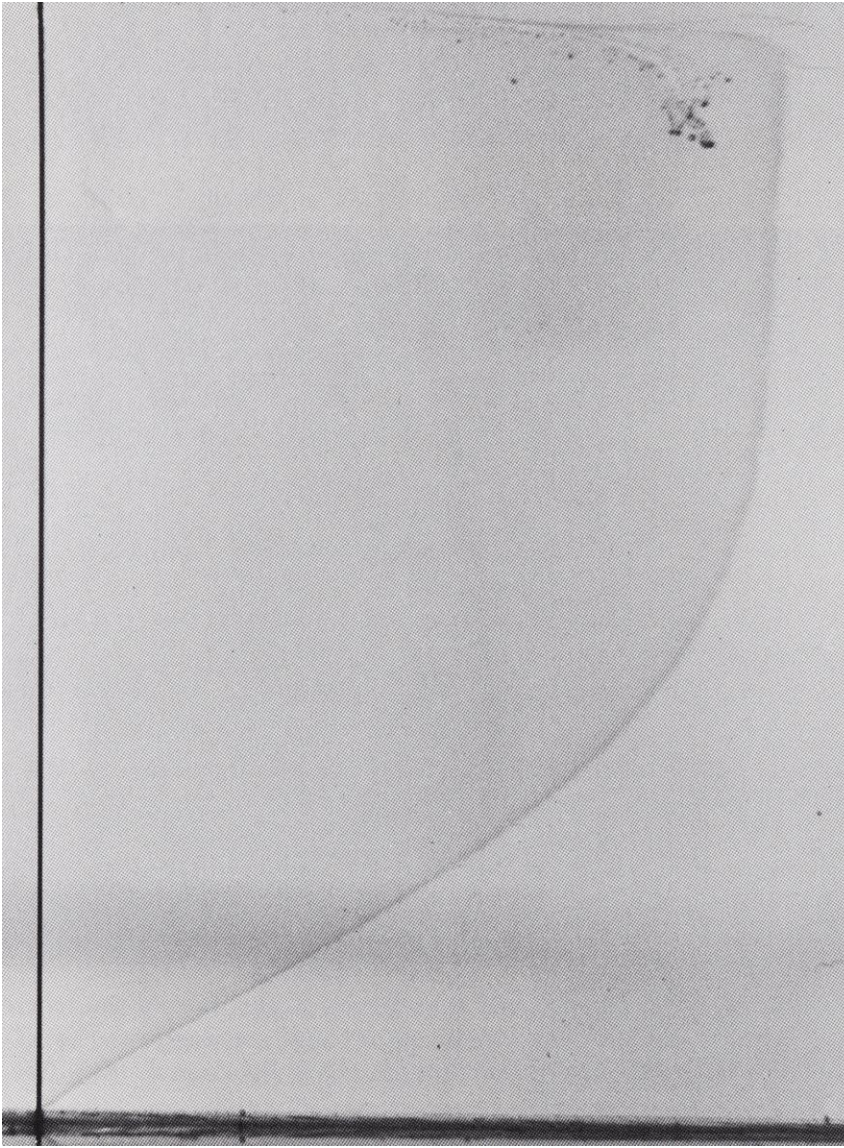
(b) A nonwetted surface

Figure 2.11



1. Hele-Shaw flow past a circle. Dye shows the streamlines in water flowing at 1 mm per second between glass plates spaced 1 mm apart. It is at first sight paradoxical that the best way of producing the unseparated pattern of plane potential flow past a bluff object, which

would be spoiled by separation in a real fluid of even the slightest viscosity, is to go to the opposite extreme of creeping flow in a narrow gap, which is dominated by viscous forces. Photograph by D. H. Peregrine

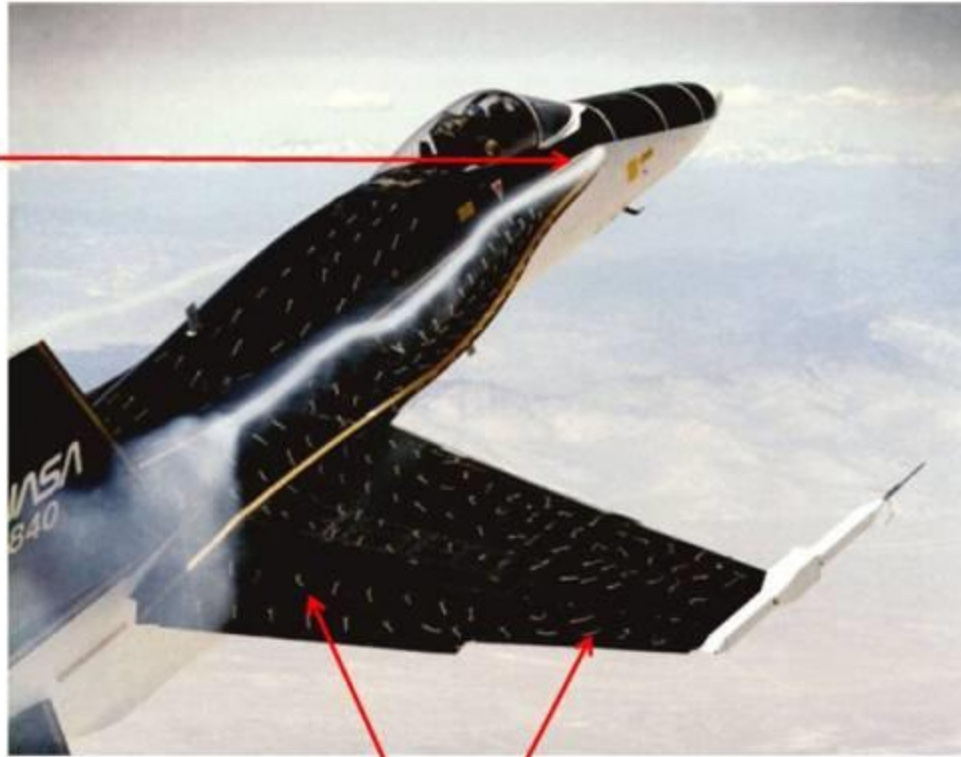


**30. Blasius boundary-layer profile on a flat plate.** The tangential velocity profile in the laminar boundary layer on a flat plate, discovered by Prandtl and calculated accurately by Blasius, is made visible by tellurium. Water is flowing at 9 cm/s. The Reynolds number is 500 based on distance from the leading edge, and the displacement thickness is about 5 mm. A fine tellurium wire perpendicular to the plate at the left is subjected to an electrical impulse of a few milliseconds duration. A chemical reaction produces a slender colloidal cloud, which drifts with the stream and is photographed a moment later to define the velocity profile. *Photograph by F. X. Wortmann*



# Smoke and Tufts

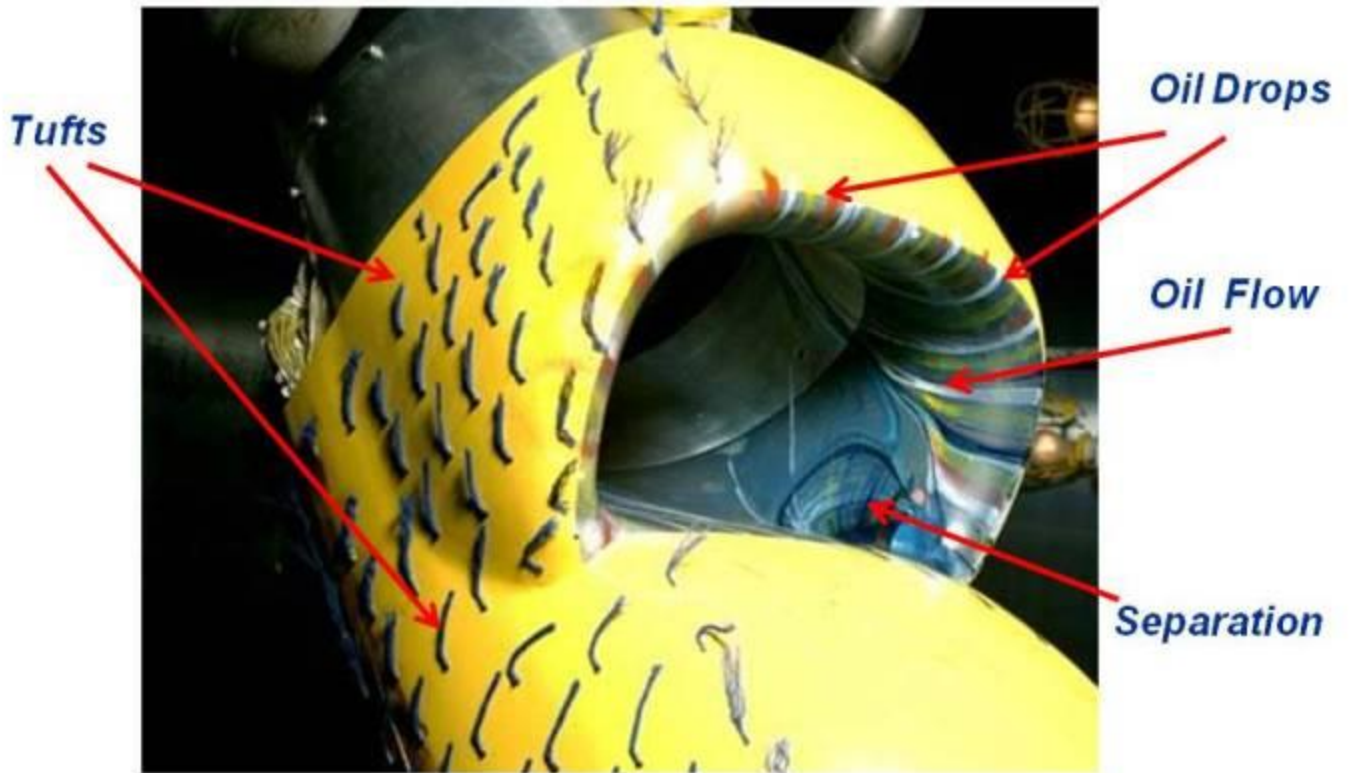
**Smoke  
Injection**



**Surface Tufts**



# Surface Oil Flow





# Laser Sheet

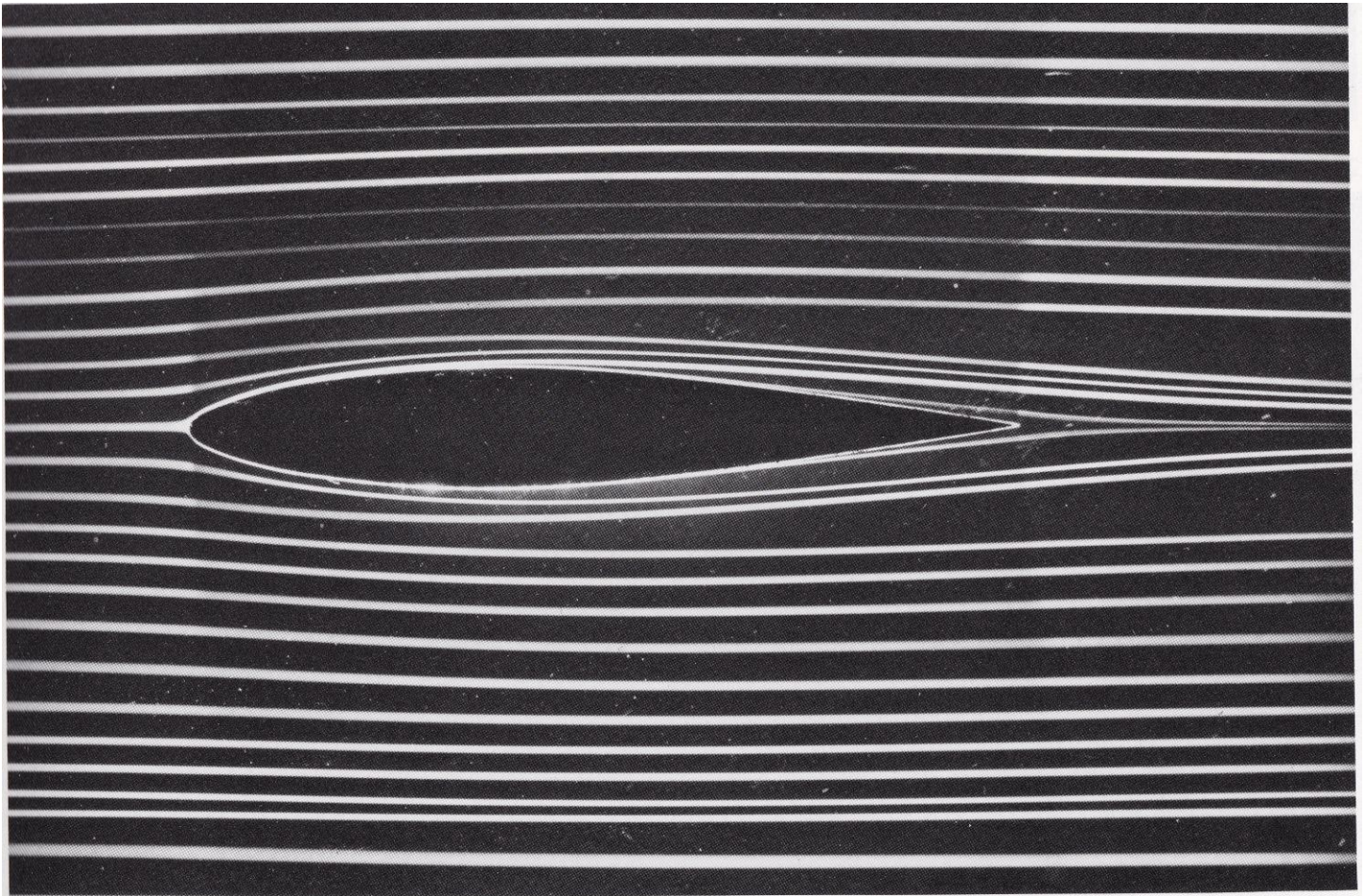
**Laser Source**



**Flow Direction  
Seed**



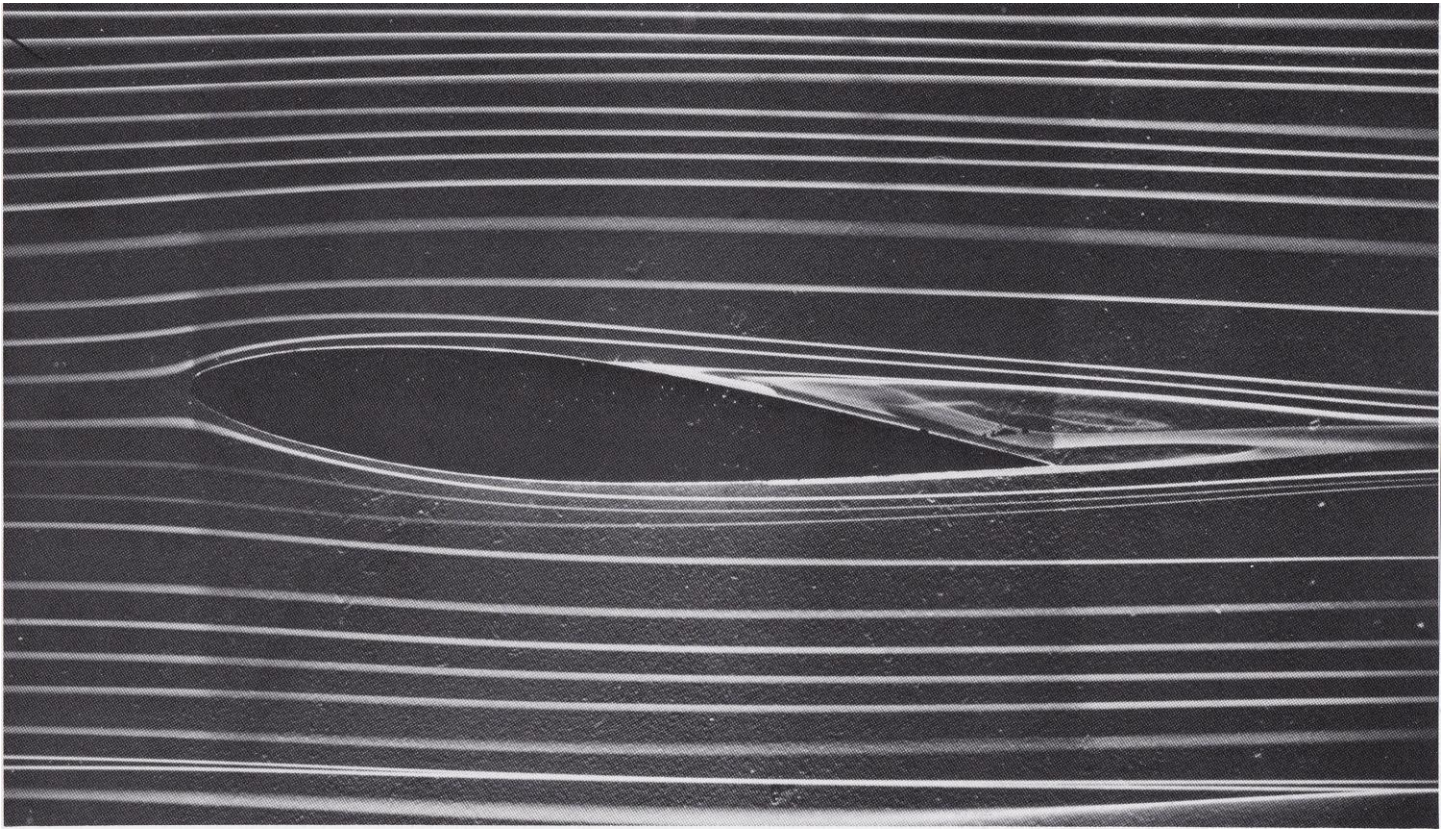
**Vortex Core**



23. **Symmetric plane flow past an airfoil.** An NACA 64A015 profile is at zero incidence in a water tunnel. The Reynolds number is 7000 based on the chordlength. Streamlines are shown by colored fluid introduced up-

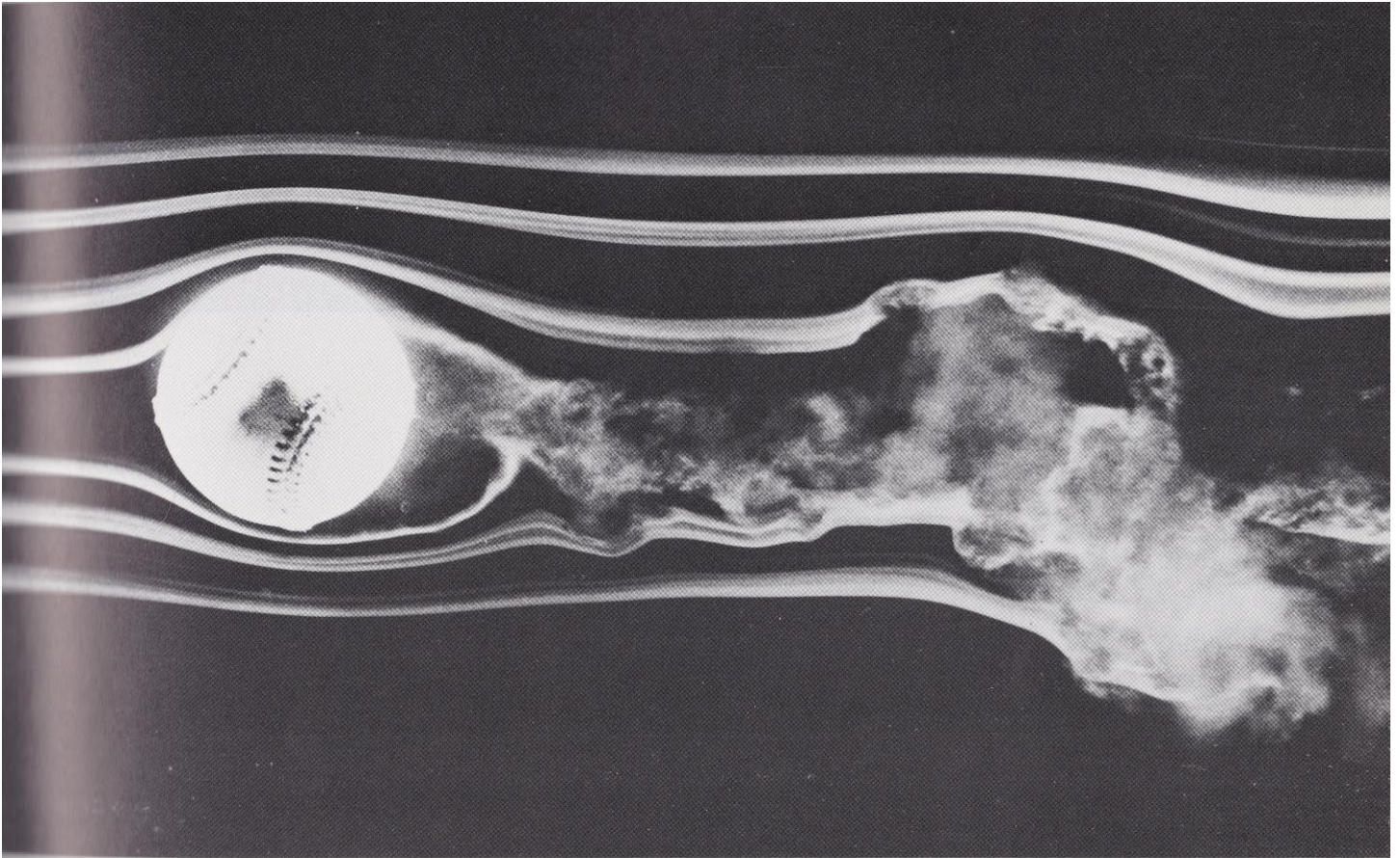
stream. The flow is evidently laminar and appears to be unseparated, though one might anticipate a small separated region near the trailing edge. *ONERA photograph, Werlé 1974*





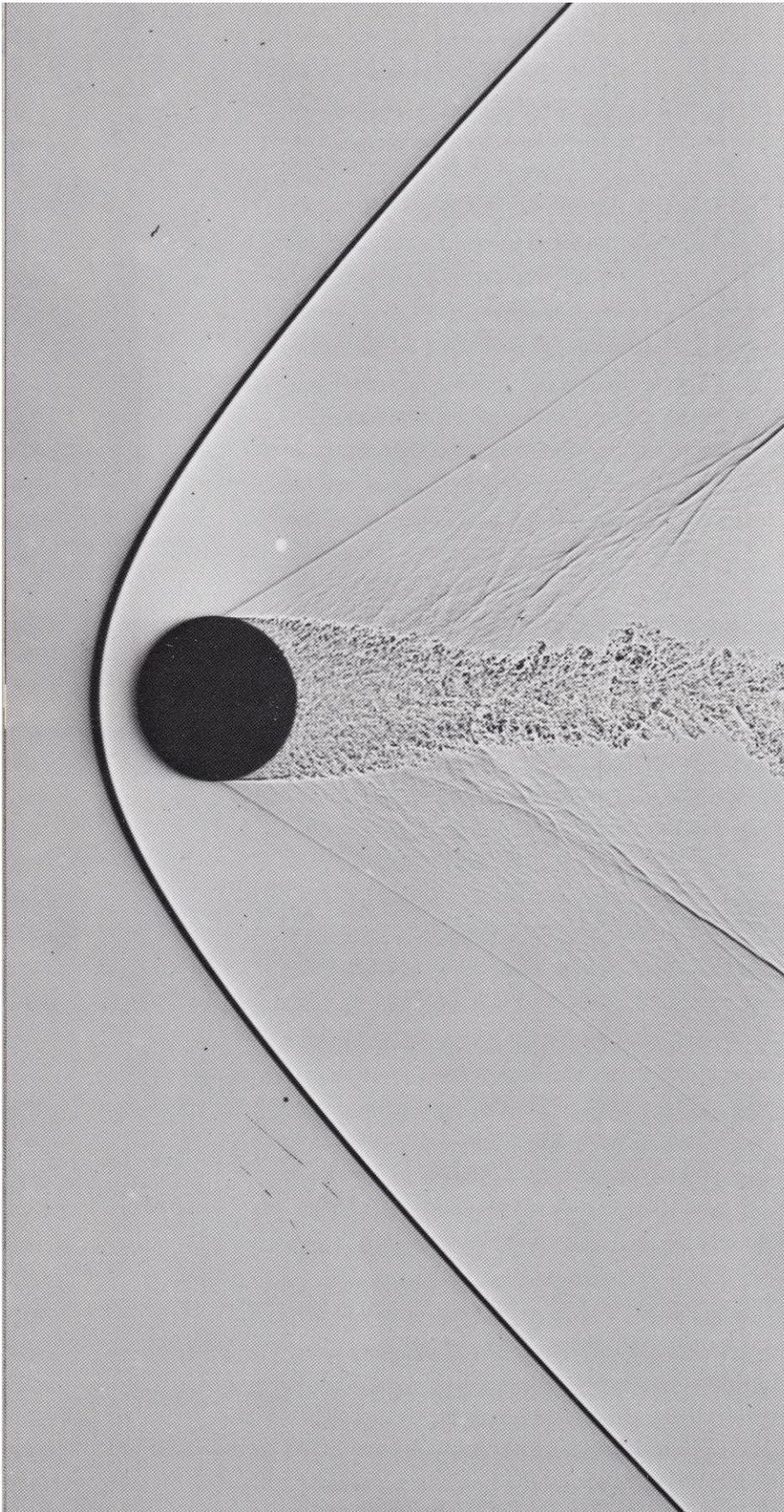
**34. Boundary-layer separation on an inclined airfoil.** When the NACA 64A015 airfoil of figure 23 is raised to  $5^\circ$  incidence the laminar boundary layer separates from the rear half of the upper surface. The flow remains attached

to the lower surface, from which it leaves tangentially at the trailing edge. Streamlines are shown by colored fluid filaments in water. ONERA photograph, Werlé 1974

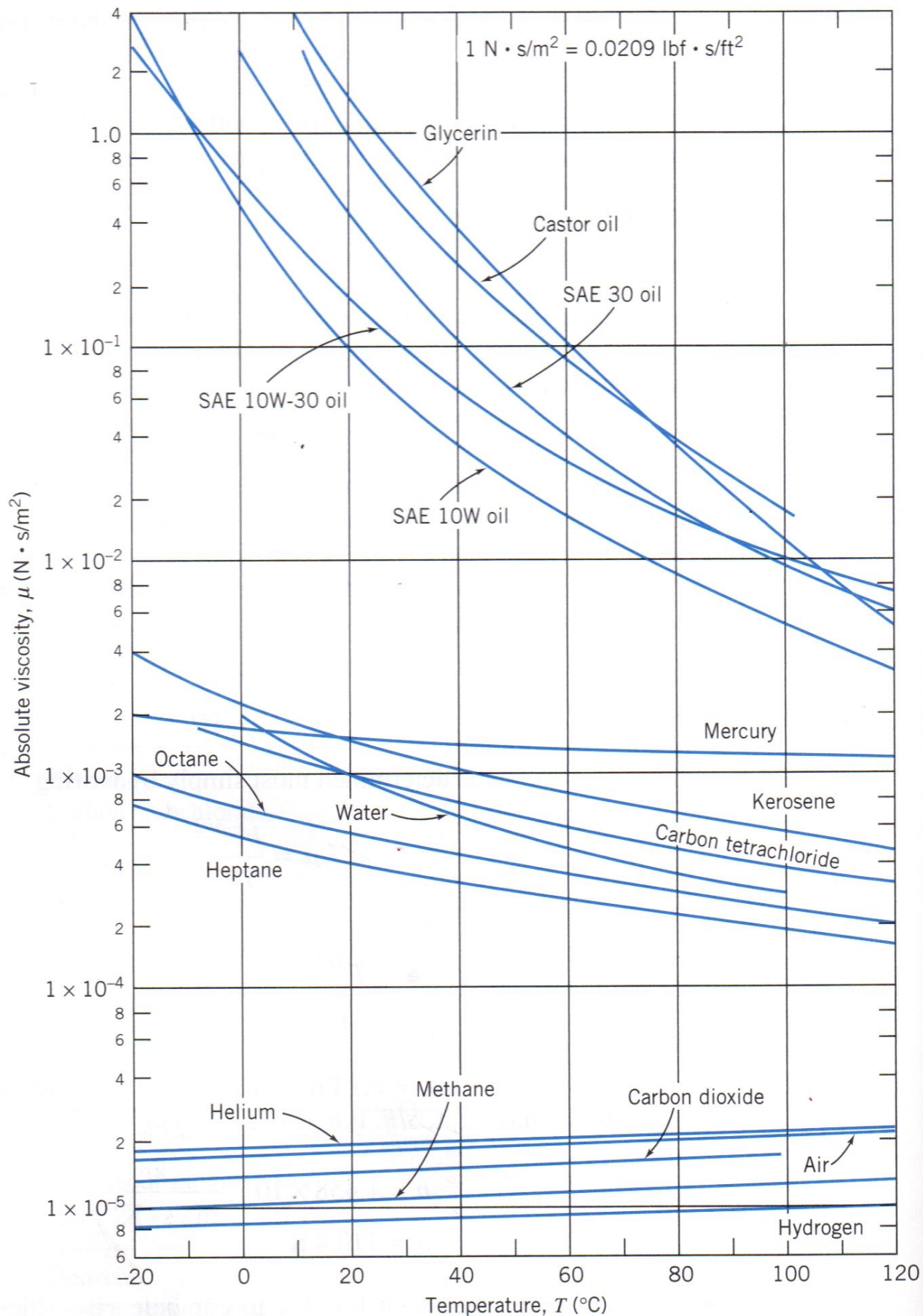


**66. Spinning baseball.** The late F. N. M. Brown devoted many years to developing and using smoke visualization in wind tunnels at the University of Notre Dame. Here the

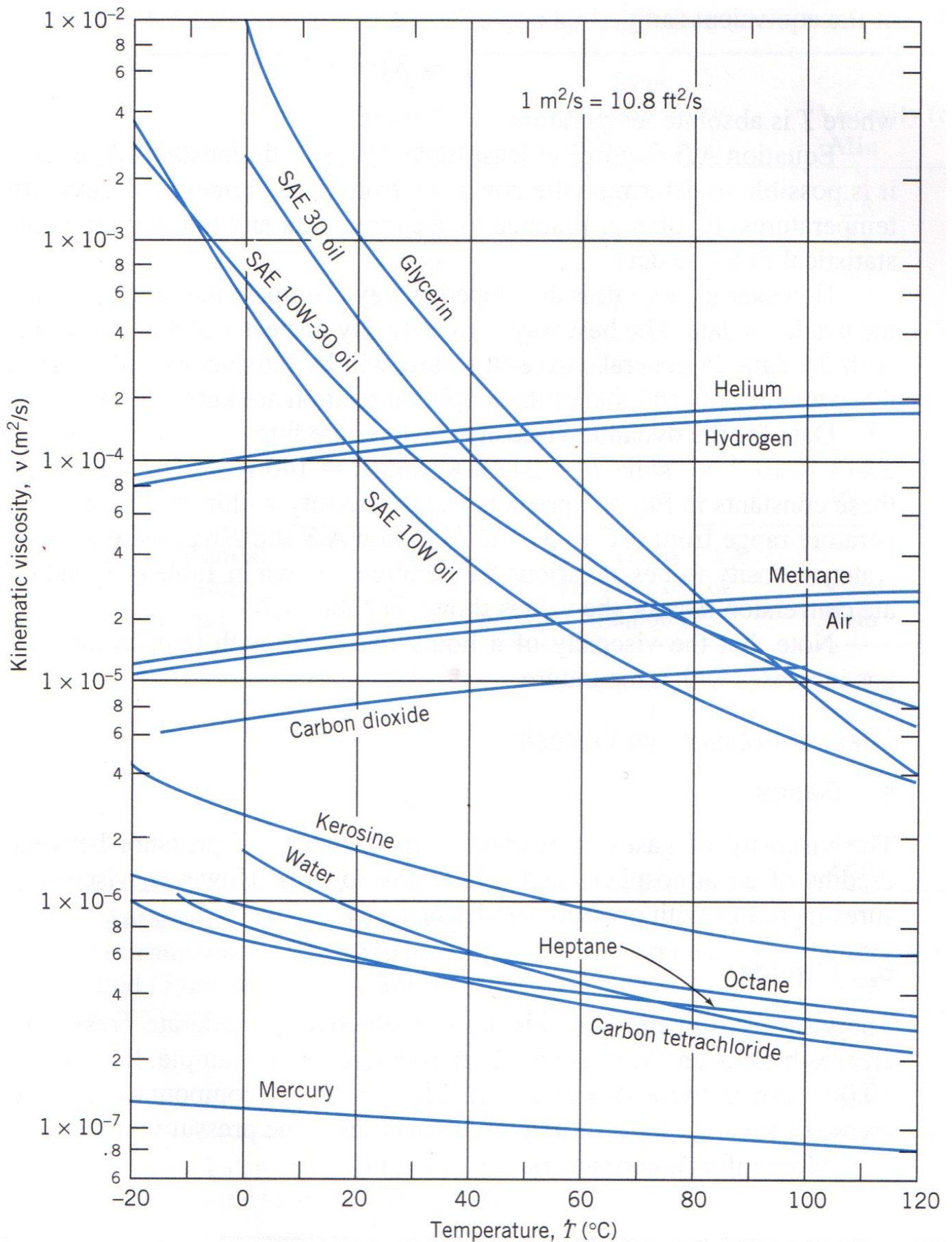
flow speed is about 77 ft/sec and the ball is rotated at 630 rpm. This unpublished photograph is similar to several in Brown 1971. *Photograph courtesy of T. J. Mueller*



**266. Sphere at  $M=1.53$ .** A shadowgraph catches a  $\frac{1}{2}$ -inch sphere in free flight through air. The flow is subsonic behind the part of the bow wave that is ahead of the sphere, and over its surface back to  $45^\circ$ . At about  $90^\circ$  the laminar boundary layer separates through an oblique shock wave, and quickly becomes turbulent. The fluctuating wake generates a system of weak disturbances that merge into the second shock wave. *Photograph by A. C. Charters*



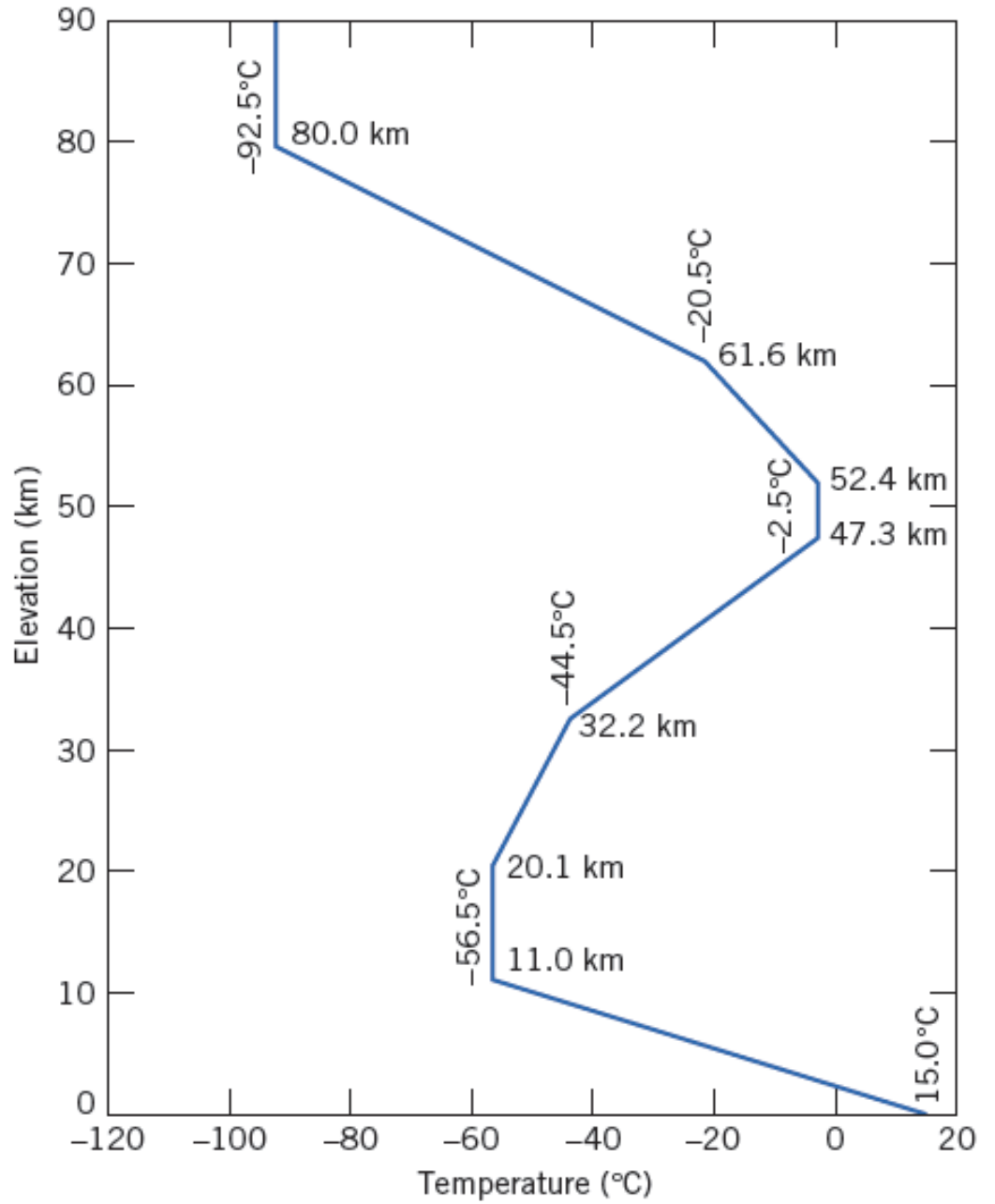
**Fig. A.2** Dynamic (absolute) viscosity of common fluids as a function of temperature. (Data from [1, 6, and 10].)



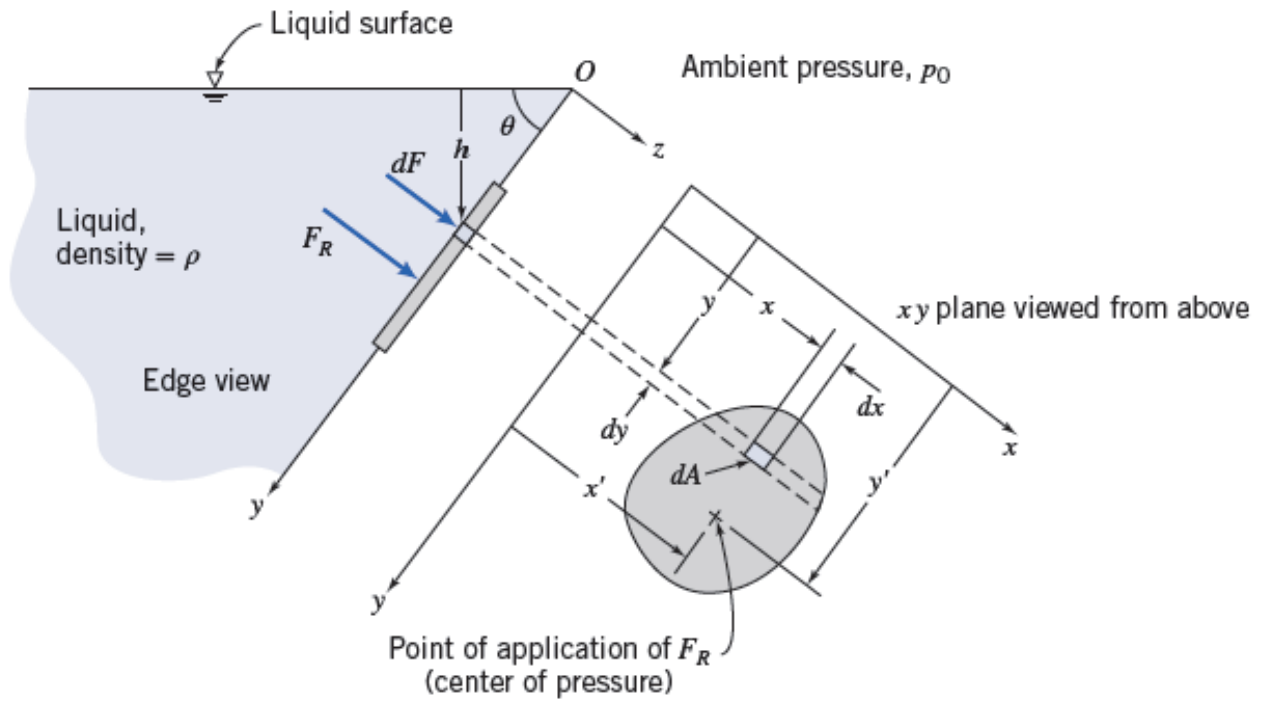
**Fig. A.3** Kinematic viscosity of common fluids (at atmospheric pressure) as a function of temperature. (Data from [1, 6, and 10].)



# CHAPTER 3



**Fig. 3.3** Temperature variation with altitude in the U.S. Standard Atmosphere.



**Fig. 3.5** Plane submerged surface.



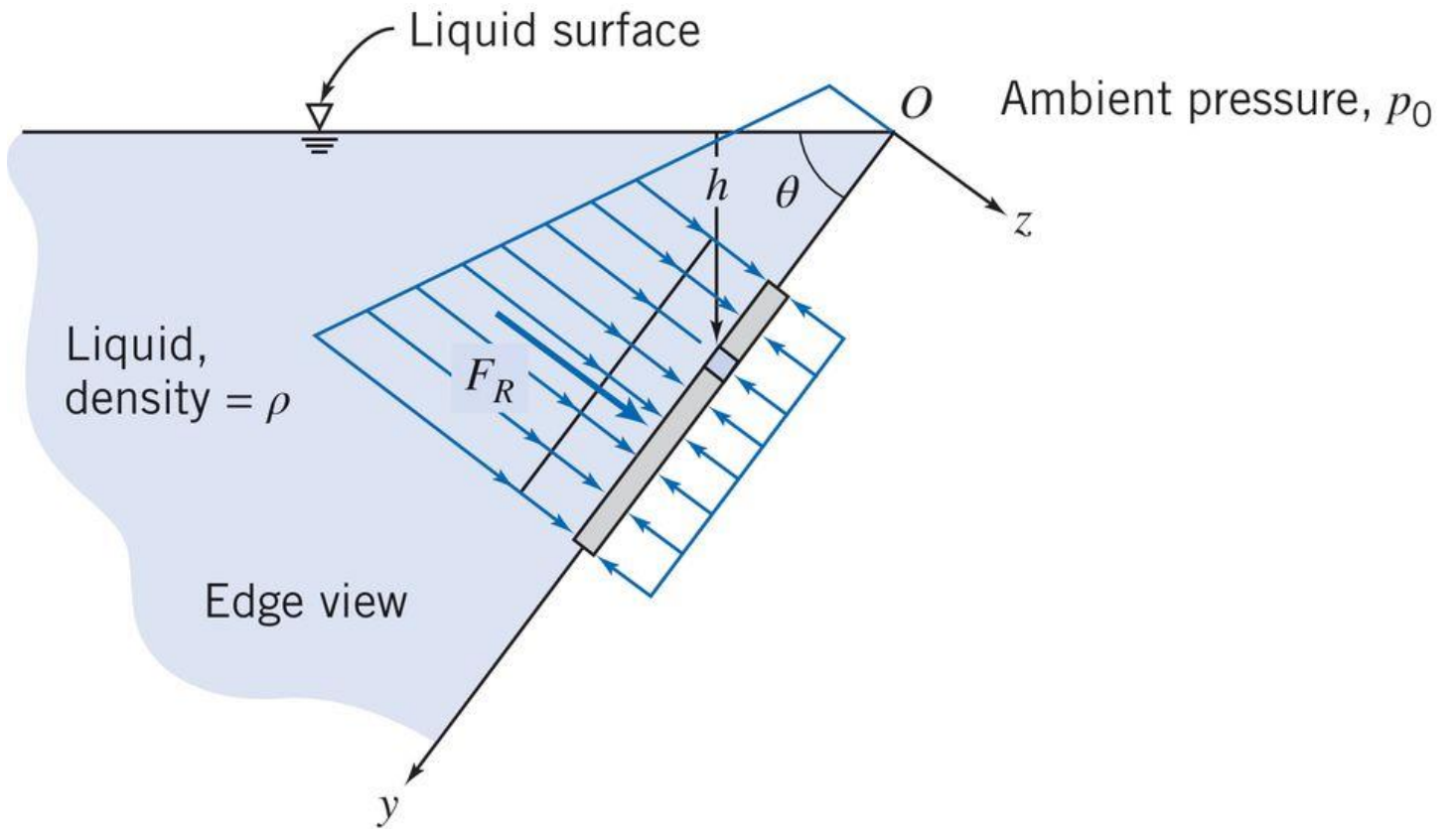
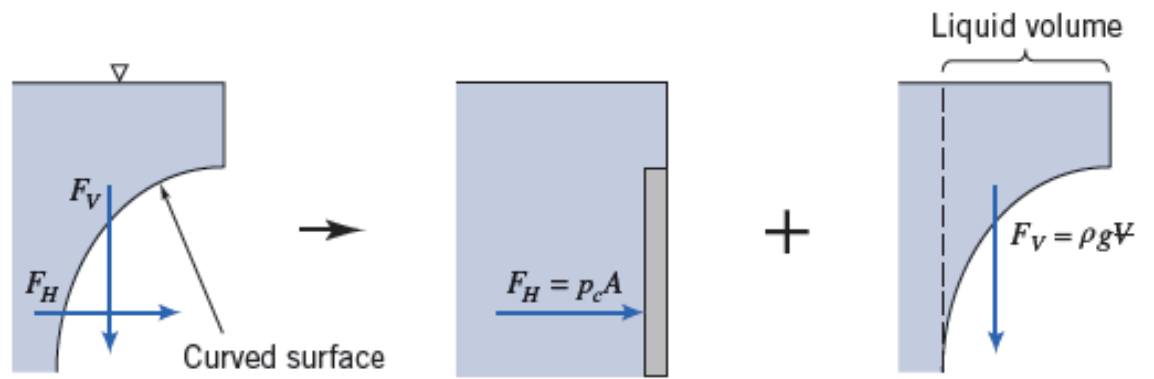
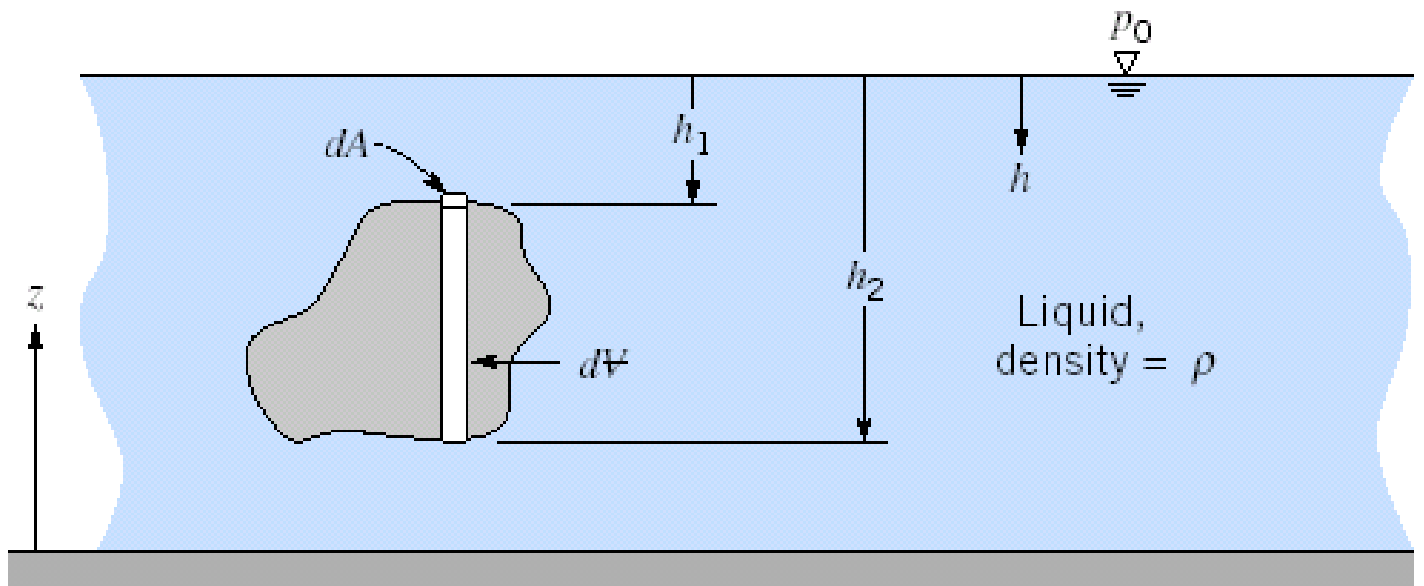


Fig. 3.6 Pressure distribution on plane submerged surface.



**Fig. 3.8** Forces on curved submerged surface.



**Fig. 3.9** Immersed body in static liquid.

Table A.3

Properties of the U.S. Standard Atmosphere

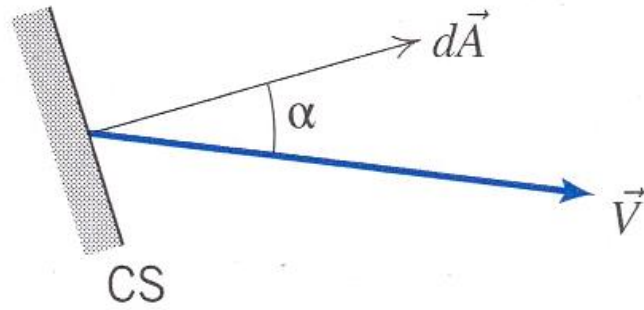
Geometric Altitude (m)	Temperature (K)	$p/p_{SL}$ (—)	$\rho/\rho_{SL}$ (—)
-500	291.4	1.061	1.049
0	288.2	1.000 <sup>a</sup>	1.000 <sup>b</sup>
500	284.9	0.9421	0.9529
1,000	281.7	0.8870	0.9075
1,500	278.4	0.8345	0.8638
2,000	275.2	0.7846	0.8217
2,500	271.9	0.7372	0.7812
3,000	268.7	0.6920	0.7423
3,500	265.4	0.6492	0.7048
4,000	262.2	0.6085	0.6689
4,500	258.9	0.5700	0.6343
5,000	255.7	0.5334	0.6012
6,000	249.2	0.4660	0.5389
7,000	242.7	0.4057	0.4817
8,000	236.2	0.3519	0.4292
9,000	229.7	0.3040	0.3813
10,000	223.3	0.2615	0.3376
11,000	216.8	0.2240	0.2978
12,000	216.7	0.1915	0.2546
13,000	216.7	0.1636	0.2176
14,000	216.7	0.1399	0.1860
15,000	216.7	0.1195	0.1590
16,000	216.7	0.1022	0.1359
17,000	216.7	0.08734	0.1162
18,000	216.7	0.07466	0.09930
19,000	216.7	0.06383	0.08489
20,000	216.7	0.05457	0.07258
22,000	218.6	0.03995	0.05266
24,000	220.6	0.02933	0.03832
26,000	222.5	0.02160	0.02797
28,000	224.5	0.01595	0.02047
30,000	226.5	0.01181	0.01503
40,000	250.4	0.002834	0.003262
50,000	270.7	0.0007874	0.0008383
60,000	255.8	0.0002217	0.0002497
70,000	219.7	0.00005448	0.00007146
80,000	180.7	0.00001023	0.00001632
90,000	180.7	0.000001622	0.000002588

Source: Data from Reference [7].

<sup>a</sup> $p_{SL} = 1.01325 \times 10^5 \text{ N/m}^2$  (abs) (=14.696 psia).

<sup>b</sup> $\rho_{SL} = 1.2250 \text{ kg/m}^3$ (=0.002377 slug/ft<sup>3</sup>).

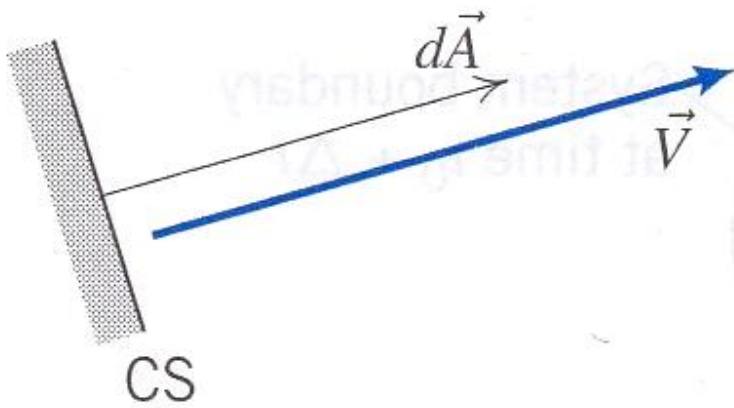
## CHAPTER 4



$$\vec{V} \cdot d\vec{A} = VdA \cos \alpha$$

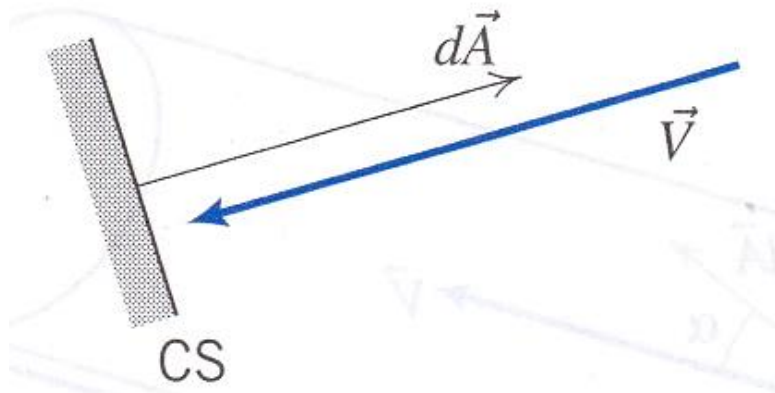
(a) General inlet/exit

**Fig. 4.3** Evaluating the scalar product.



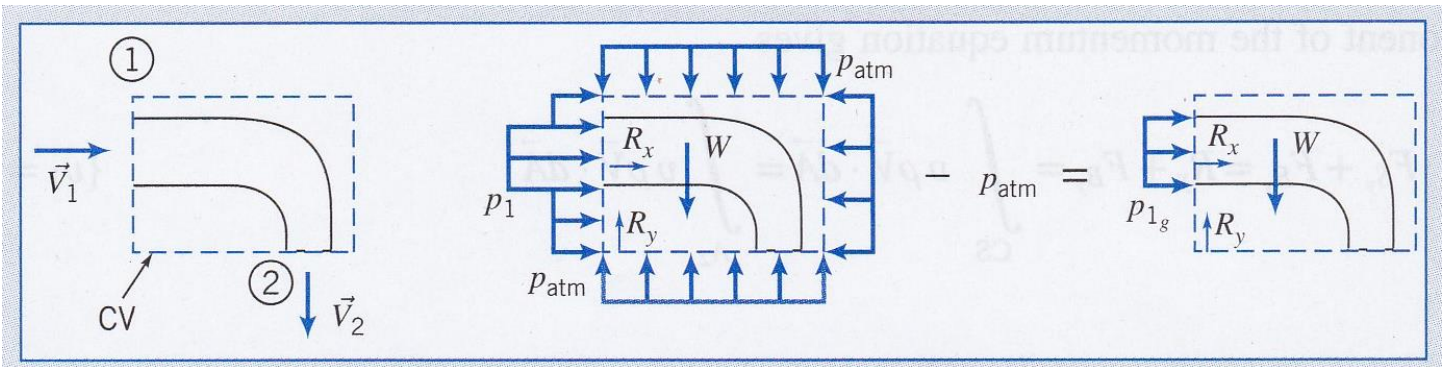
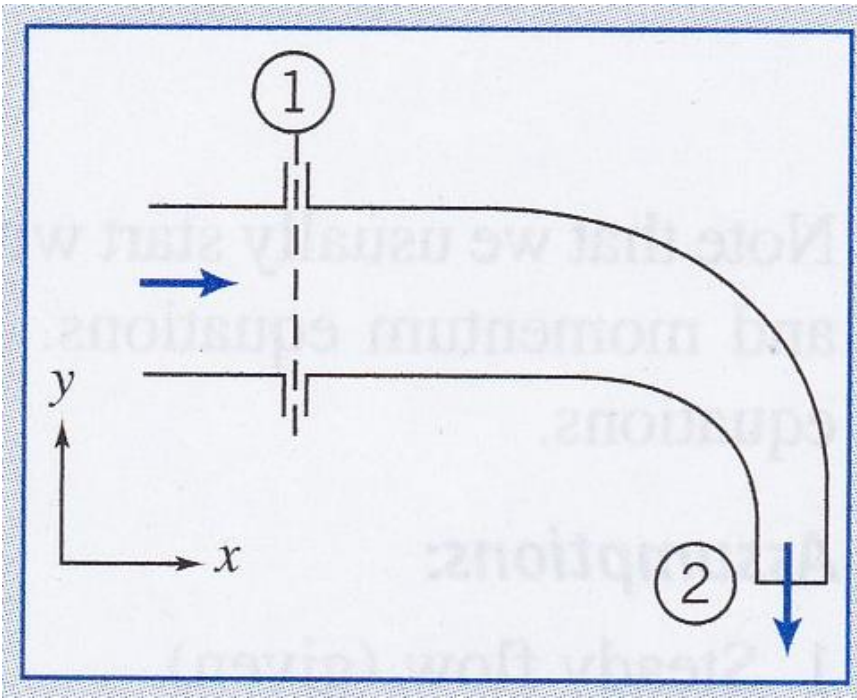
$$\vec{V} \cdot d\vec{A} = +VdA$$

(b) Normal exit



$$\vec{V} \cdot d\vec{A} = -VdA$$

(c) Normal inlet



# CHAPTER 7

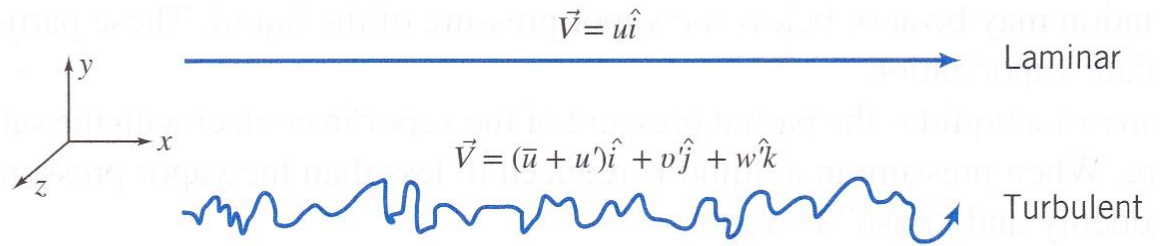
Handwritten musical notation on a five-line staff, showing a series of connected, wavy lines.

Handwritten musical notation on a five-line staff, showing a series of connected, wavy lines.

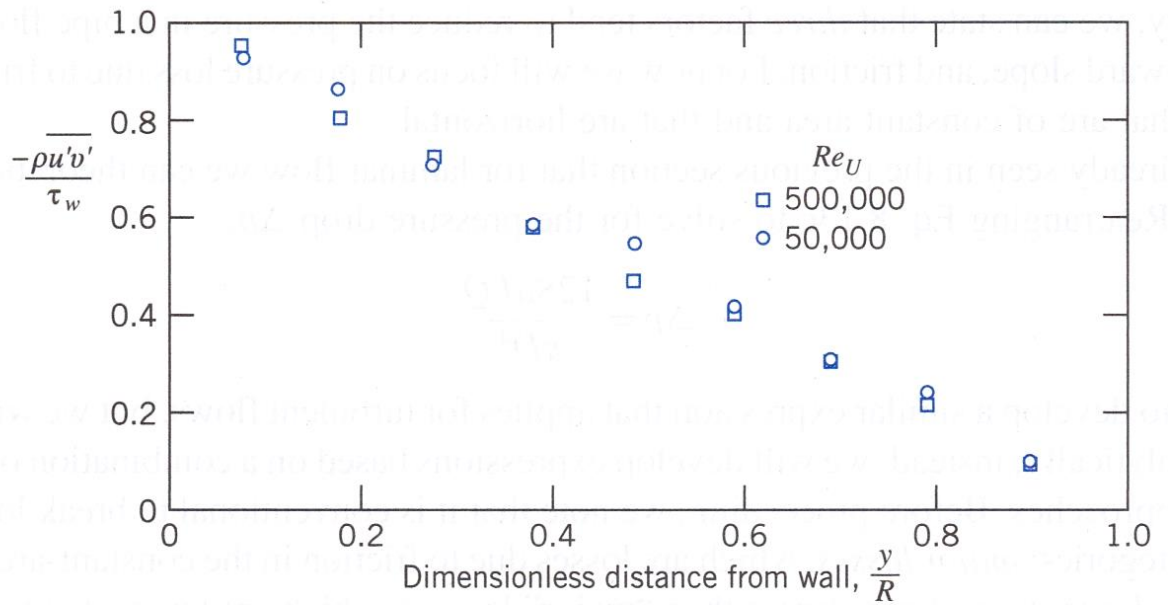
Handwritten musical notation on a five-line staff, showing a series of connected, wavy lines.



# CHAPTER 8



**Fig. 2.17** Particle pathlines in one-dimensional laminar and turbulent flows.



**Fig. 8.8** Turbulent shear stress (Reynolds stress) for fully developed turbulent flow in a pipe. (Data from [1])

159. Sublayer of a turbulent boundary layer. A suspension of aluminum particles in a stream of water shows the streaks in the sublayer of a turbulent boundary layer on a flat wall. A mirror is used to show a simultaneous side view. Cantwell, Coles & Dimotakis 1978

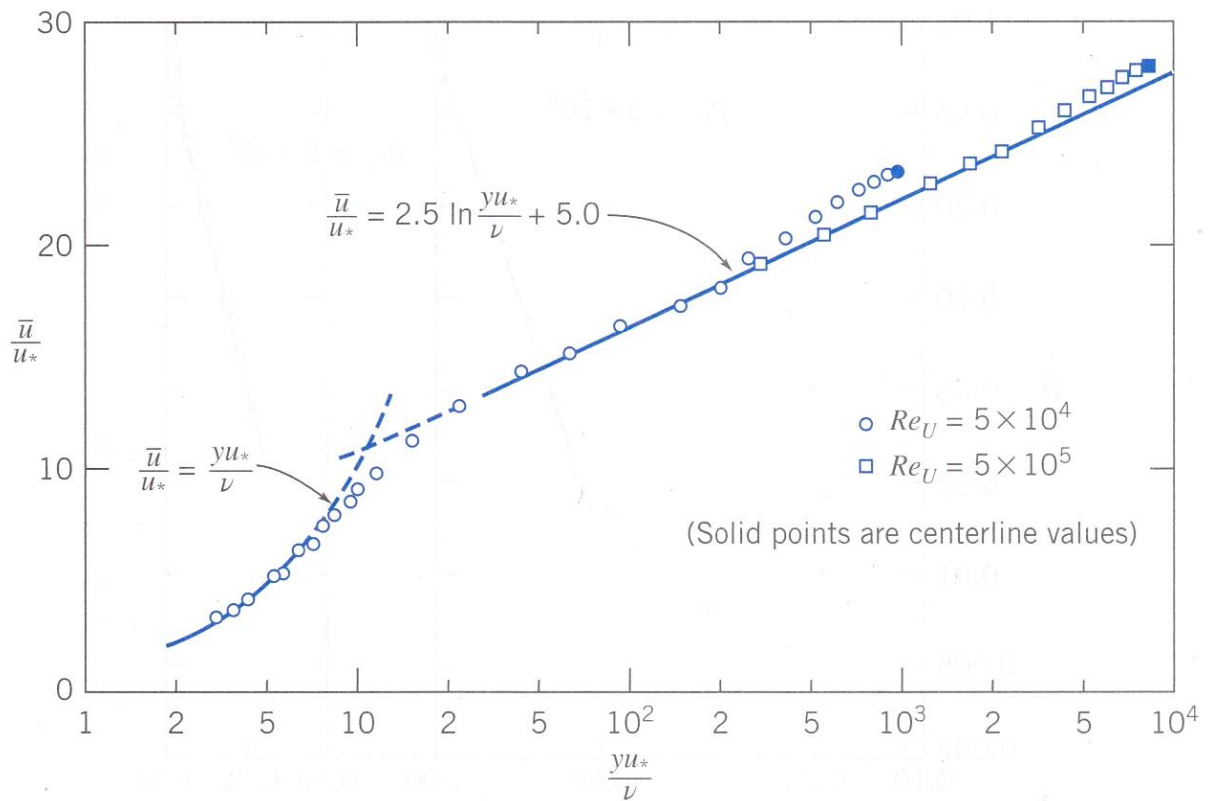
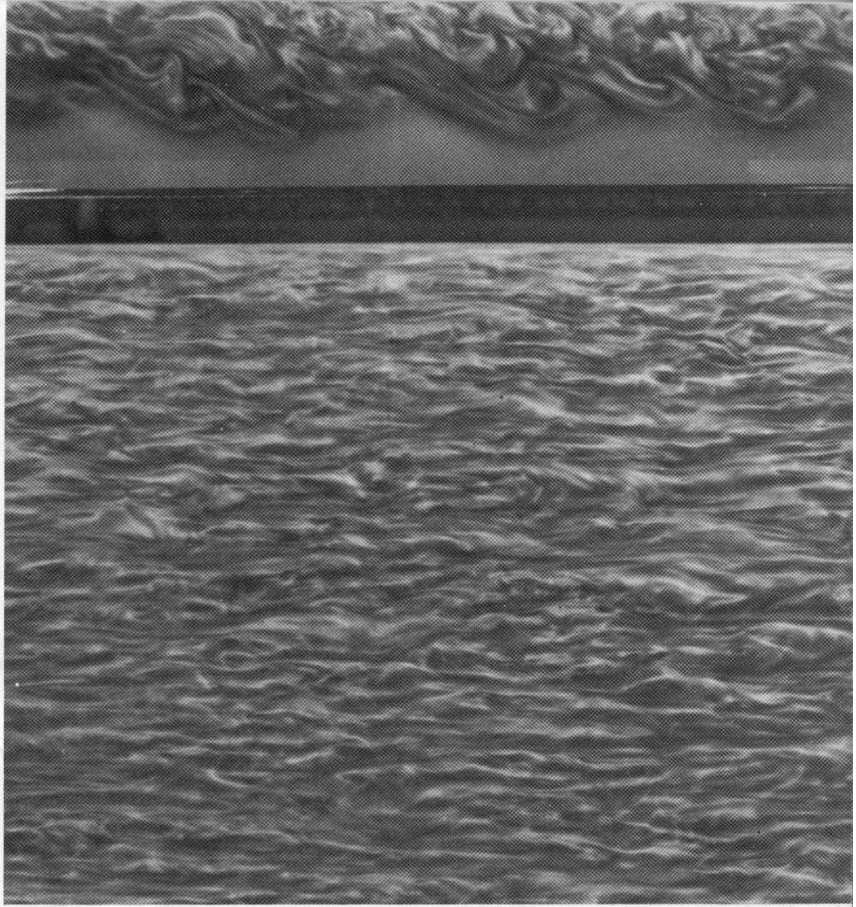
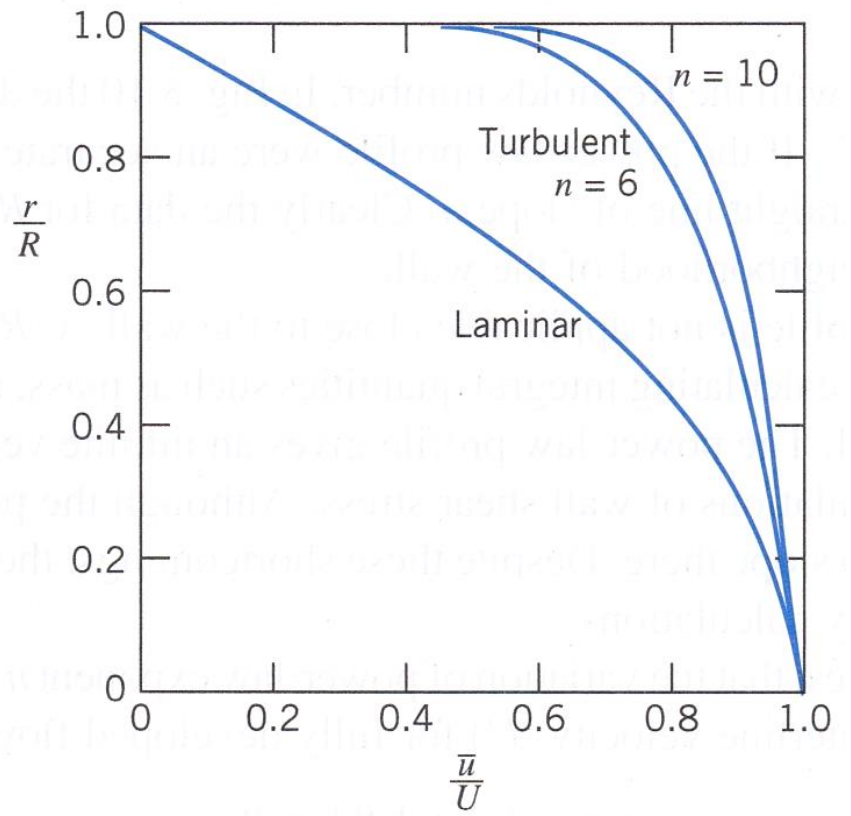
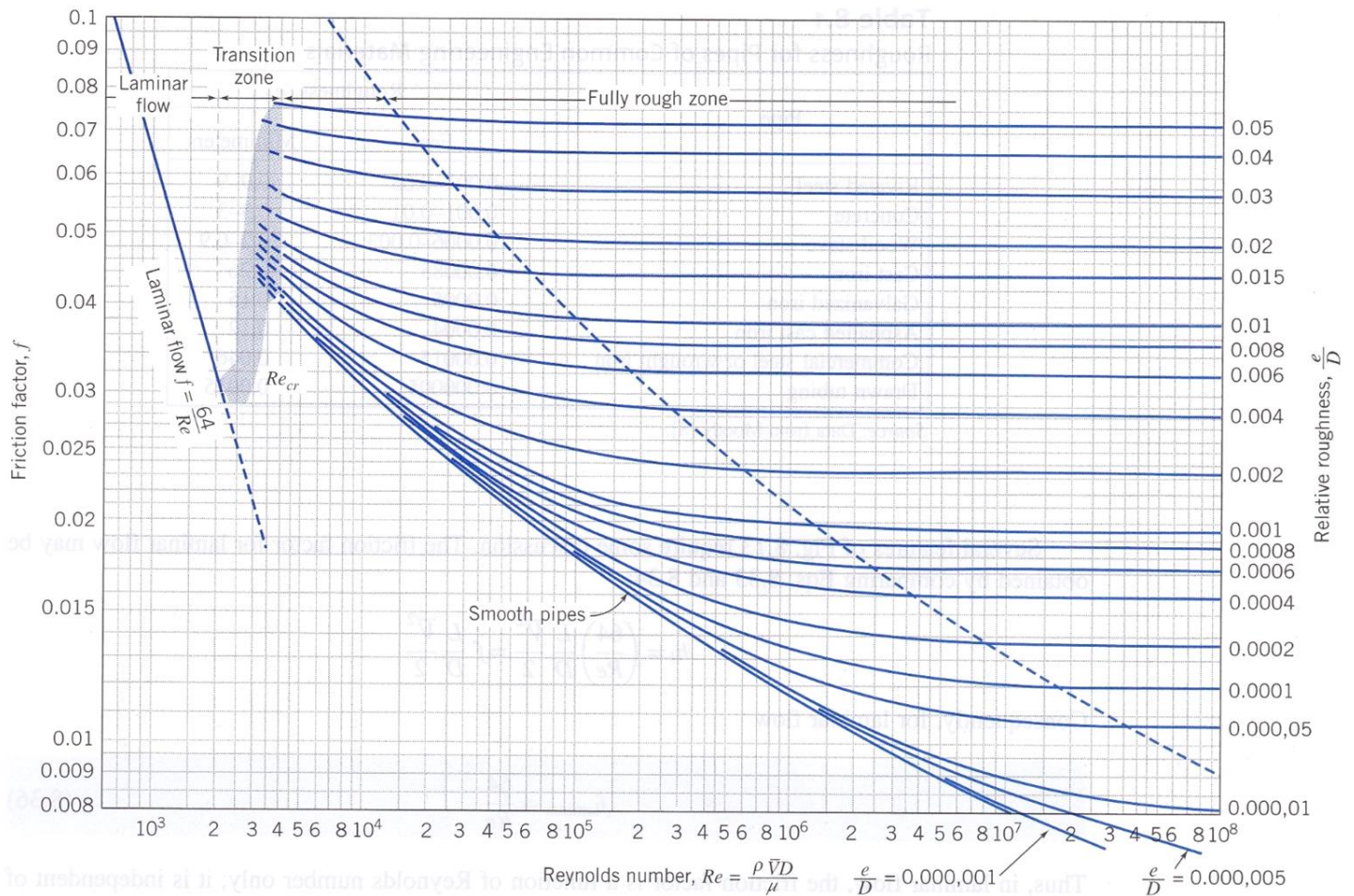


Fig. 8.9 Turbulent velocity profile for fully developed flow in a smooth pipe. (Data from Laufer [5].)



**Fig. 8.11** Velocity profiles for fully developed pipe flow.



**Fig. 8.13** Friction factor for fully developed flow in circular pipes. (Data from Moody [8].)

## Table 8.1

### Roughness for Pipes of Common Engineering Materials

Pipe	Roughness, $e$	
	Feet	Millimeters
Riveted steel	0.003–0.03	0.9–9
Concrete	0.001–0.01	0.3–3
Wood stave	0.0006–0.003	0.2–0.9
Cast iron	0.00085	0.26
Galvanized iron	0.0005	0.15
Asphalted cast iron	0.0004	0.12
Commercial steel or wrought iron	0.00015	0.046
Drawn tubing	0.000005	0.0015

Source: Data from Moody [8].

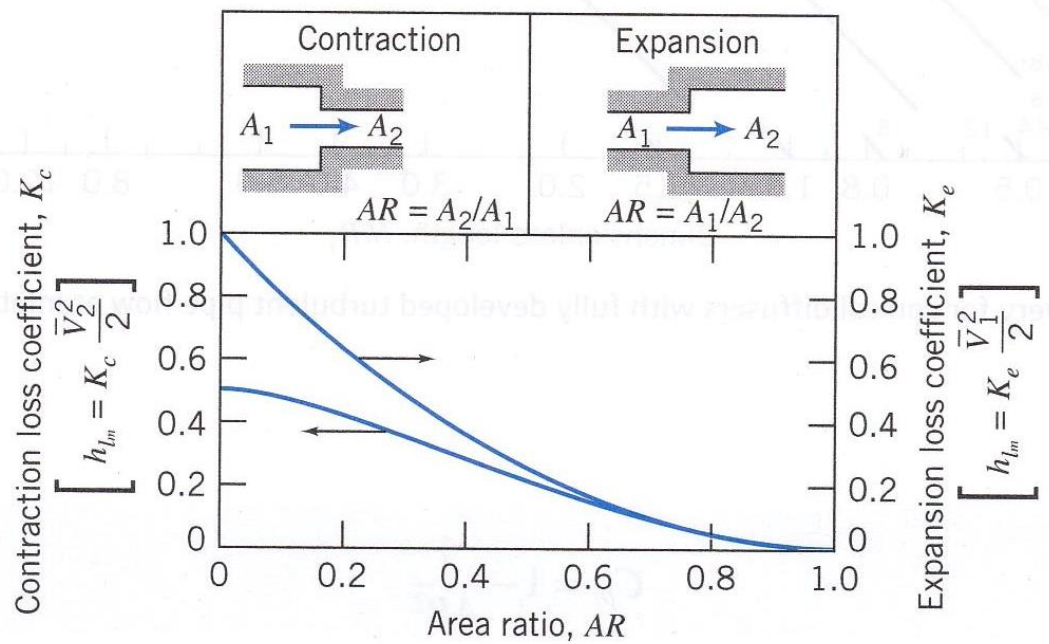
**Table 8.2**

**Minor Loss Coefficients for Pipe Entrances**

Entrance Type		Minor Loss Coefficient, $K^a$								
Reentrant		0.5 – 1.0 (depending on length of pipe entrance)								
Square-edged		0.5								
Rounded		<table border="1"> <thead> <tr> <th><math>r/D</math></th> <th><math>K</math></th> </tr> </thead> <tbody> <tr> <td>0.02</td> <td>0.3</td> </tr> <tr> <td>0.06</td> <td>0.2</td> </tr> <tr> <td><math>\geq 0.15</math></td> <td>0.04</td> </tr> </tbody> </table>	$r/D$	$K$	0.02	0.3	0.06	0.2	$\geq 0.15$	0.04
$r/D$	$K$									
0.02	0.3									
0.06	0.2									
$\geq 0.15$	0.04									

<sup>a</sup> Based on  $h_{lm} = K(\bar{V}^2/2)$ , where  $\bar{V}$  is the mean velocity in the pipe.

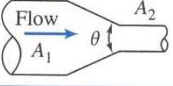
Source: Data from Reference [12].



**Fig. 8.15** Loss coefficients for flow through sudden area changes. (Data from Streeter [1].)

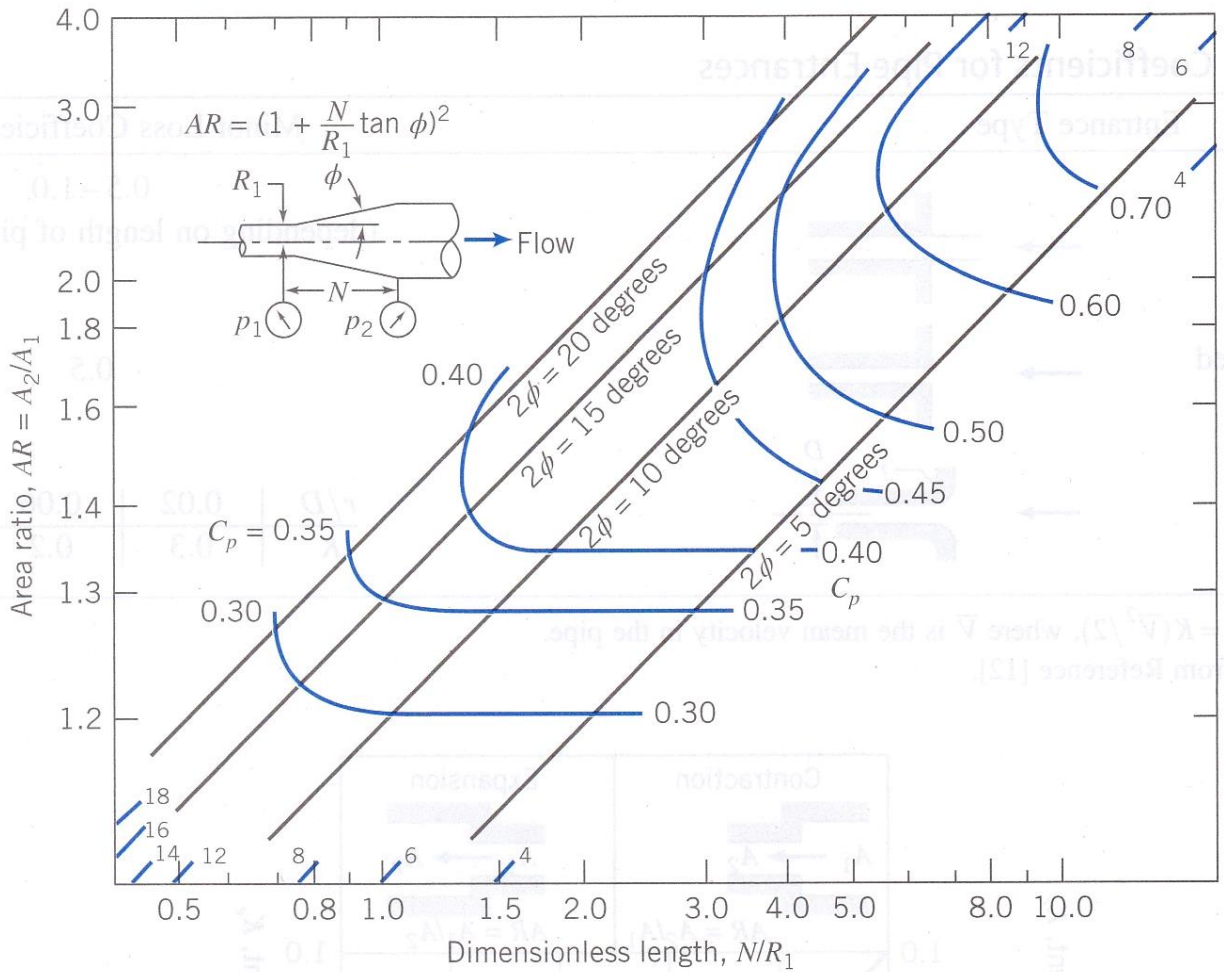
**Table 8.3**

Loss Coefficients ( $K$ ) for Gradual Contractions: Round and Rectangular Ducts

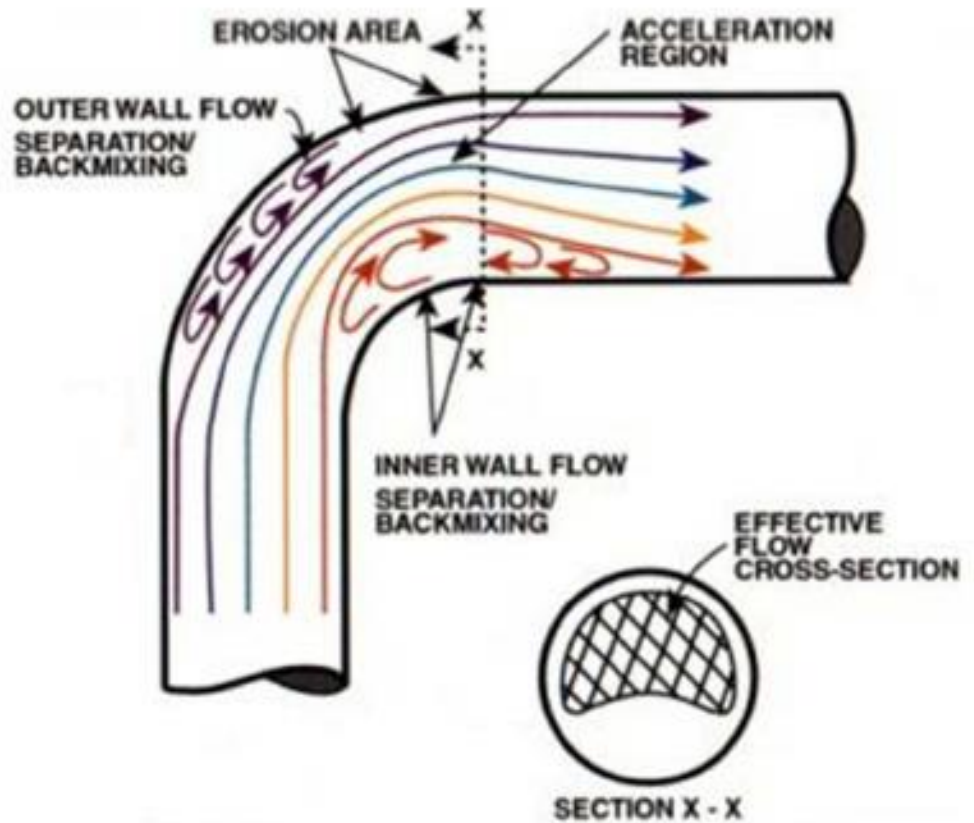
	Included Angle, $\theta$ , Degrees							
	$A_2/A_1$	10	15-40	50-60	90	120	150	180
	0.50	0.05	0.05	0.06	0.12	0.18	0.24	0.26
	0.25	0.05	0.04	0.07	0.17	0.27	0.35	0.41
	0.10	0.05	0.05	0.08	0.19	0.29	0.37	0.43

Note: Coefficients are based on  $h_{lm} = K(\bar{V}_2^2/2)$ .

Source: Data from ASHRAE [12].



**Fig. 8.16** Pressure recovery for conical diffusers with fully developed turbulent pipe flow at inlet. (Data from Bradley [13].)



**Figure 1.** Flow separation inside an elbow

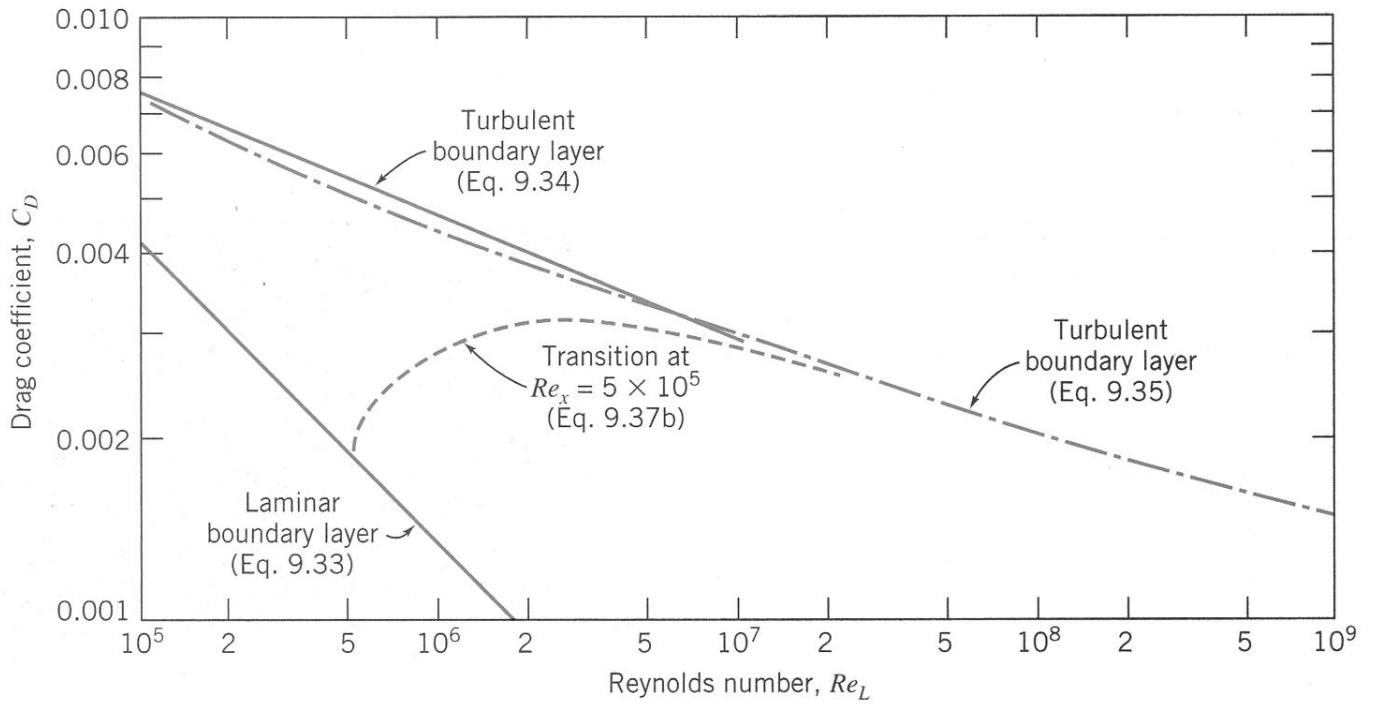
**Table 8.4**

Representative Loss Coefficients for Fittings and Valves

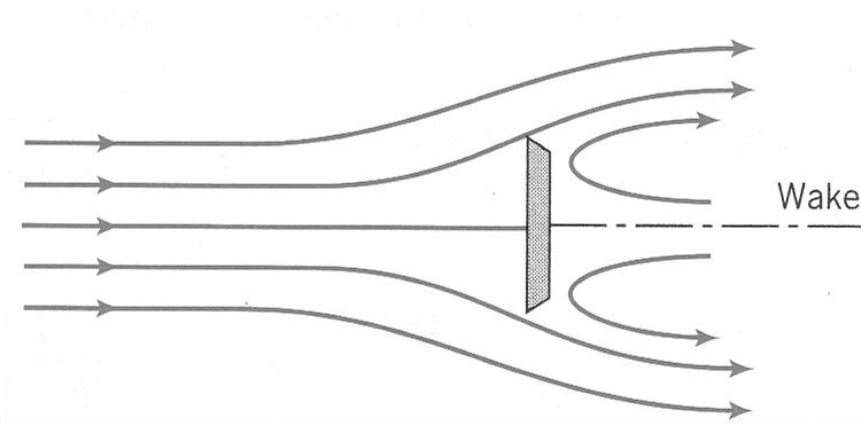
Fitting	Geometry	$K$	Fitting	Geometry	$K$
90° elbow	Flanged regular	0.3	Globe valve	Open	10
	Flanged long radius	0.2	Angle valve	Open	5
	Threaded regular	1.5	Gate valve	Open	0.20
	Threaded long radius	0.7		75% open	1.10
	Miter	1.30		50% open	3.6
45° Elbow	Miter with vanes	0.20		25% open	28.8
	Threaded regular	0.4	Ball valve	Open	0.5
	Flanged long radius	0.2		1/3 closed	5.5
Tee, dividing line flow	Threaded	0.9		2/3 closed	200
	Flanged	0.2	Water meter		7
Tee, branching flow	Threaded	2.0	Coupling		0.08
	Flanged	1.0			

Source: Data from References [12] and [34].

## CHAPTER 9

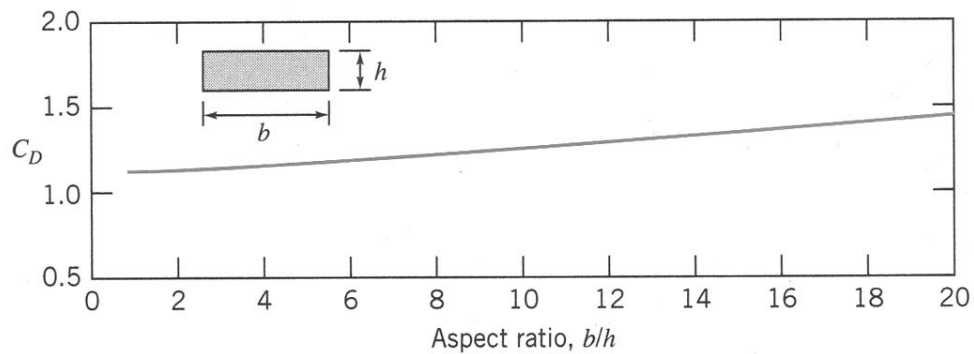


**Fig. 9.8** Variation of drag coefficient with Reynolds number for a smooth flat plate parallel to the flow.



**Fig. 9.9** Flow over a flat plate normal to the flow.

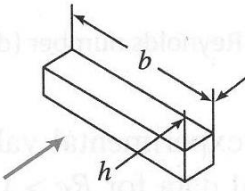



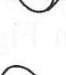
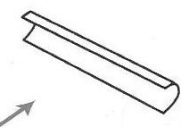
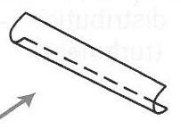




**Fig. 9.10** Variation of drag coefficient with aspect ratio for a flat plate of finite width normal to the flow with  $Re_h > 1000$  [16].

**Table 9.3**

**Drag Coefficient Data for Selected Objects ( $Re \geq 10^3$ )<sup>4</sup>**

Object	Diagram	$C_D (Re \geq 10^3)$
Square prism	 $b/h = \infty$ $b/h = 1$	2.05 1.05
Disk		1.17
Ring		1.20 <sup>b</sup>
Hemisphere (open end facing flow)		1.42
Hemisphere (open end facing downstream)		0.38
C-section (open side facing flow)		2.30
C-section (open side facing downstream)		1.20

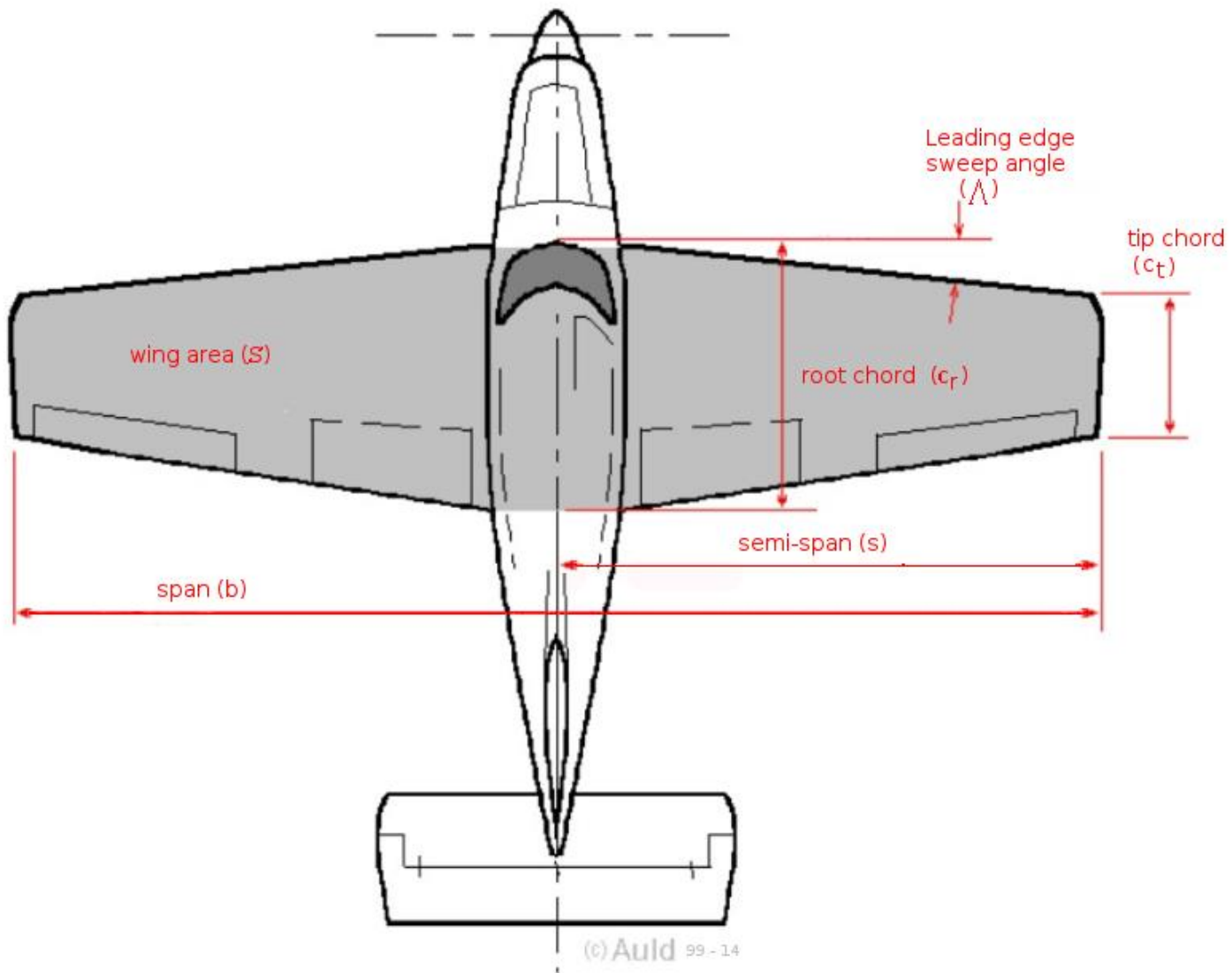


*TW-141*

*image-3*









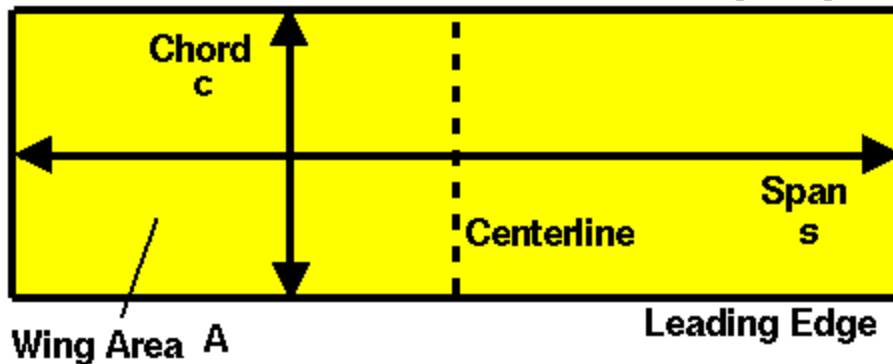
# Wing Geometry Definitions

Glenn  
Research  
Center

Top View

Wing Platform

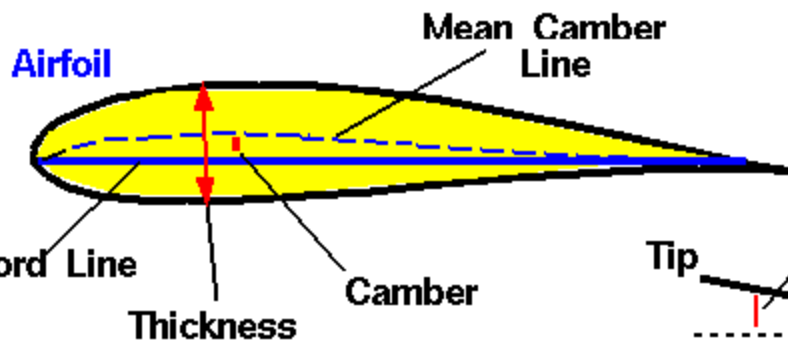
Trailing Edge



Aspect Ratio = AR

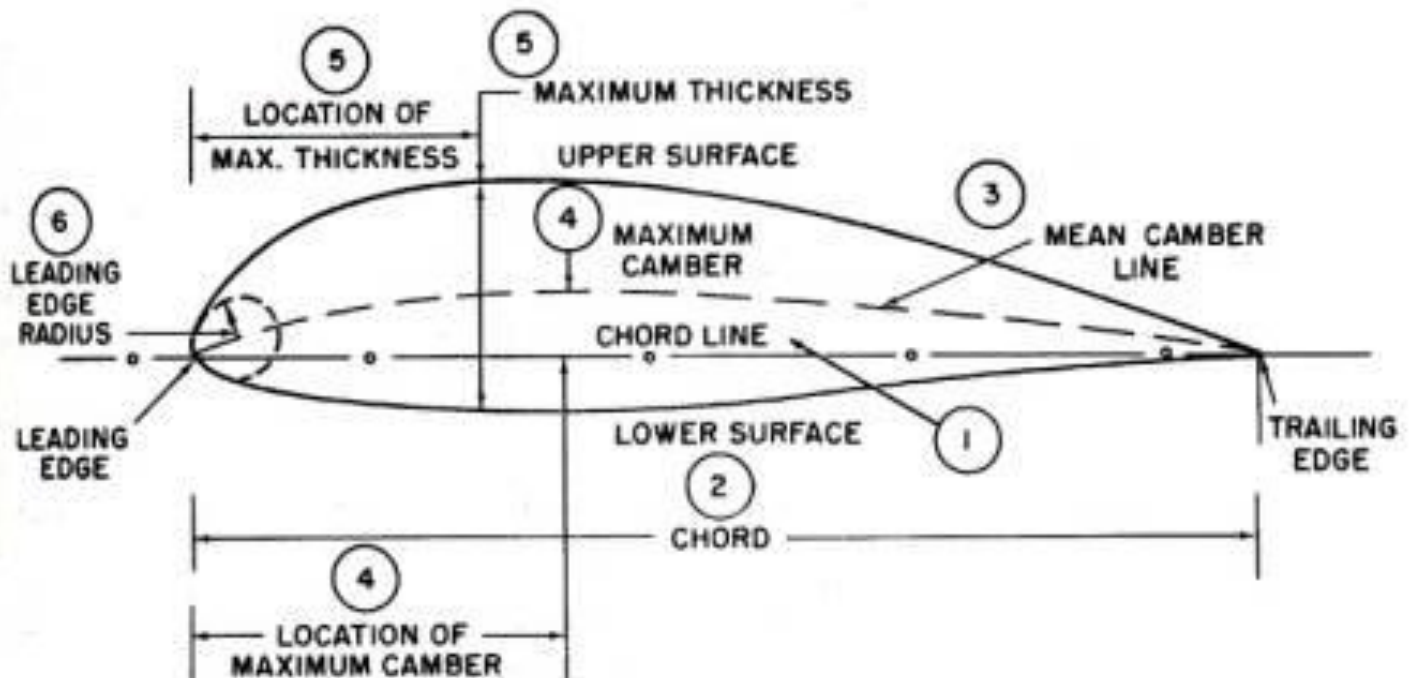
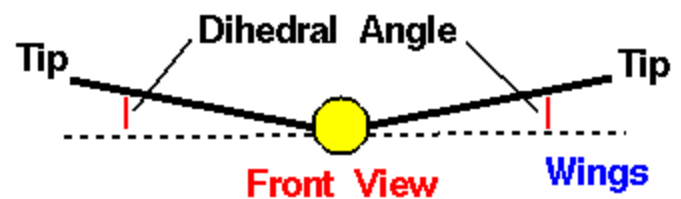
$$AR = \frac{s^2}{A}$$

$$AR = \frac{s}{c} \text{ for rectangle}$$



Symmetric Airfoil

Side View



## CONVENTIONAL AIRFOILS

The following illustrations depict a selection of designs of airfoil sections. These are known as conventional airfoils.



Low camber — low drag — high speed — thin wing section  
Suitable for race planes, fighters, interceptors, etc.



Deep camber — high lift — low speed — thick wing section  
Suitable for transports, freighters, bombers, etc.



Deep camber — high lift — low speed — thin wing section  
Suitable as above.



Low lift — high drag — reflex trailing edge wing section.  
Very little movement of centre of pressure. Good stability.

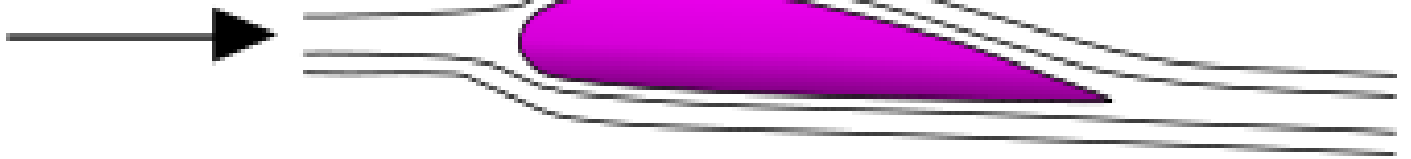


Symmetrical (cambered top and bottom) wing sections.  
Similar to above.

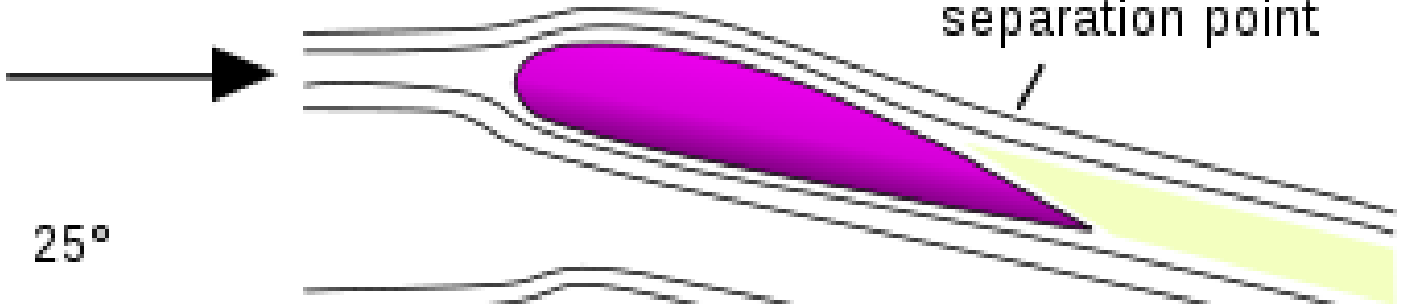


GA(W)-1 airfoil — thicker for better structure and lower weight  
— good stall characteristics — camber is maintained farther rearward which increases lifting capability over more of the airfoil and decreases drag.

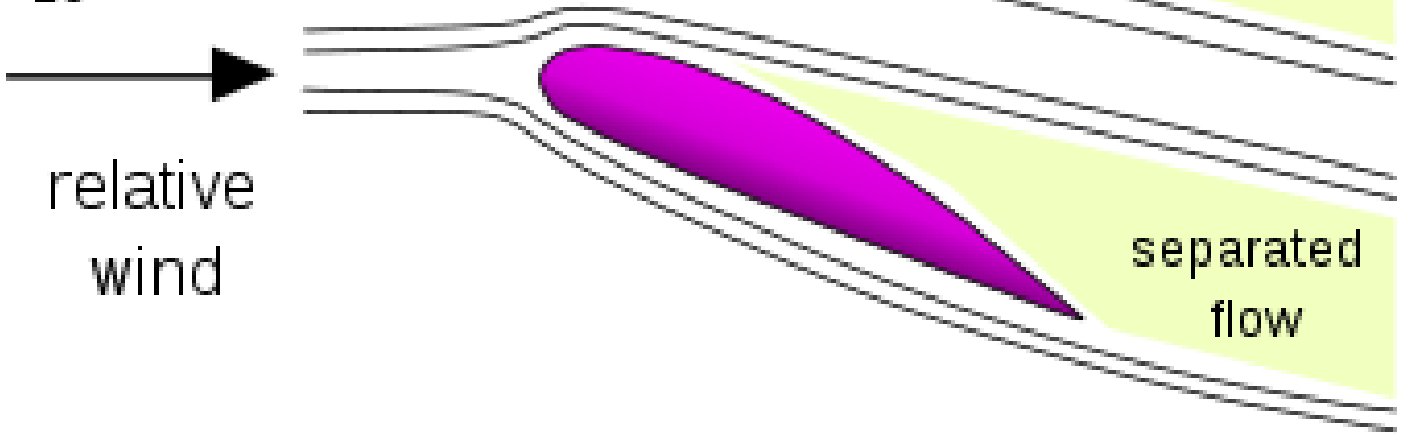
6°, steady flow



15°, stall point, maximum lift



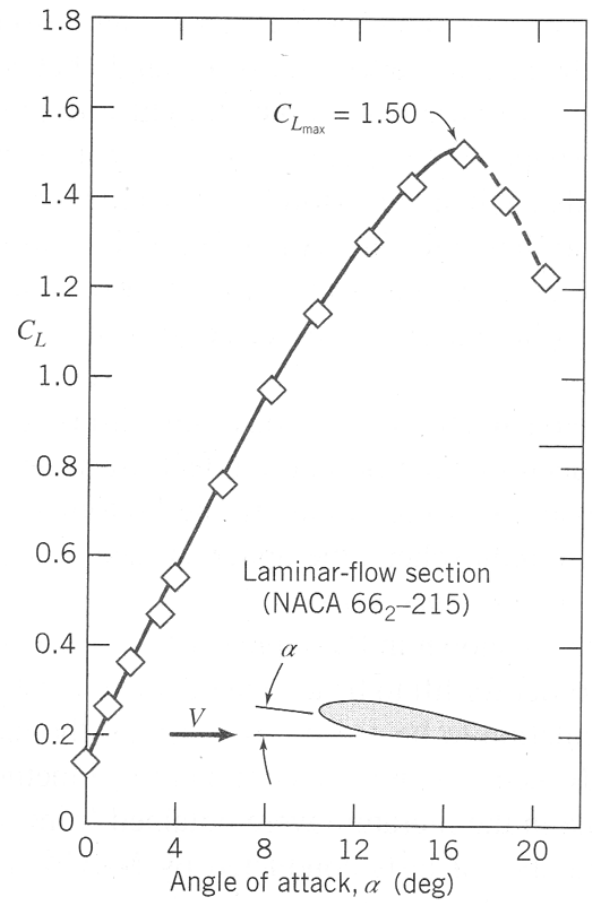
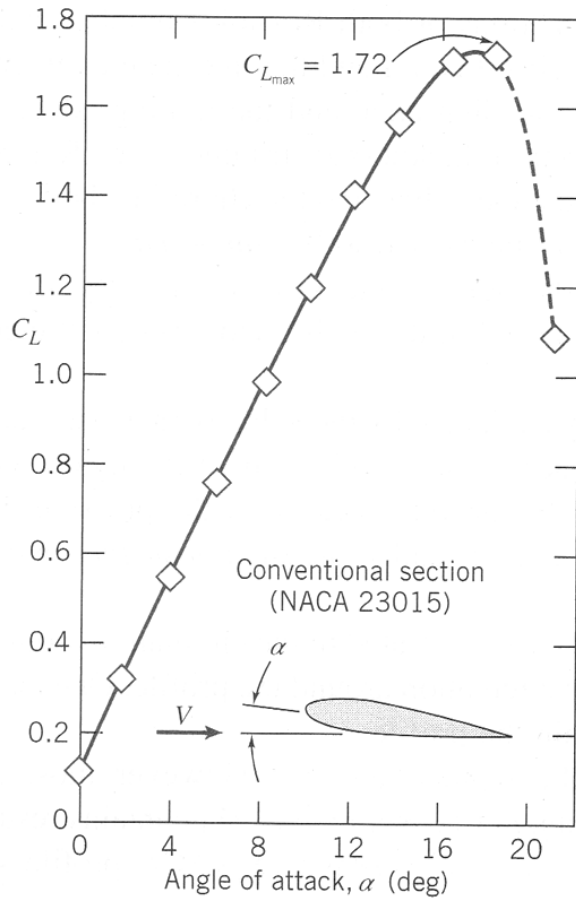
25°



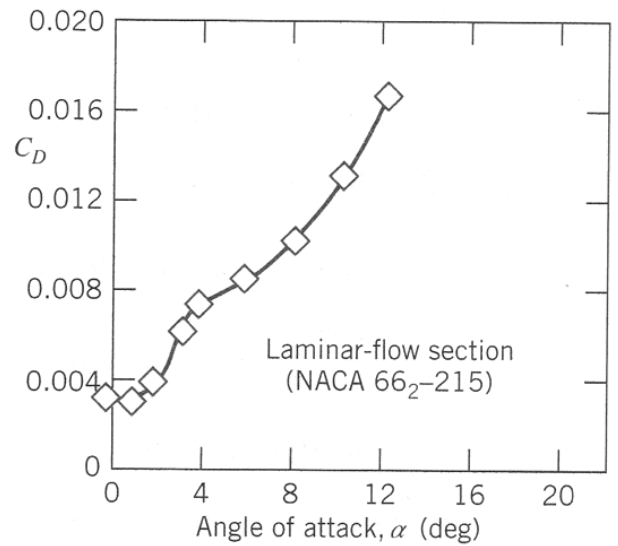
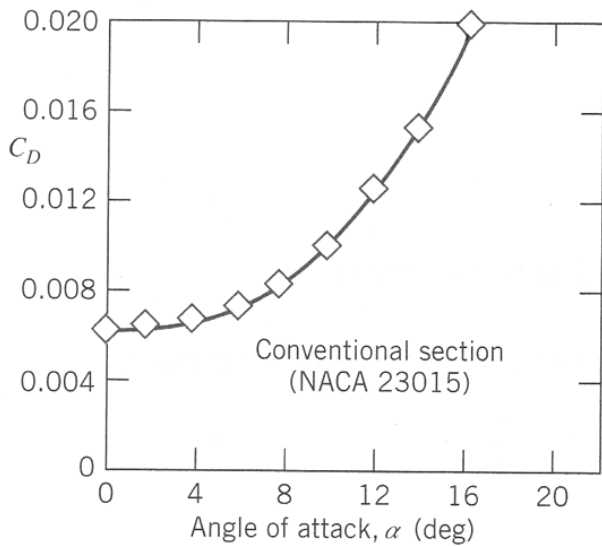
relative  
wind

separated  
flow



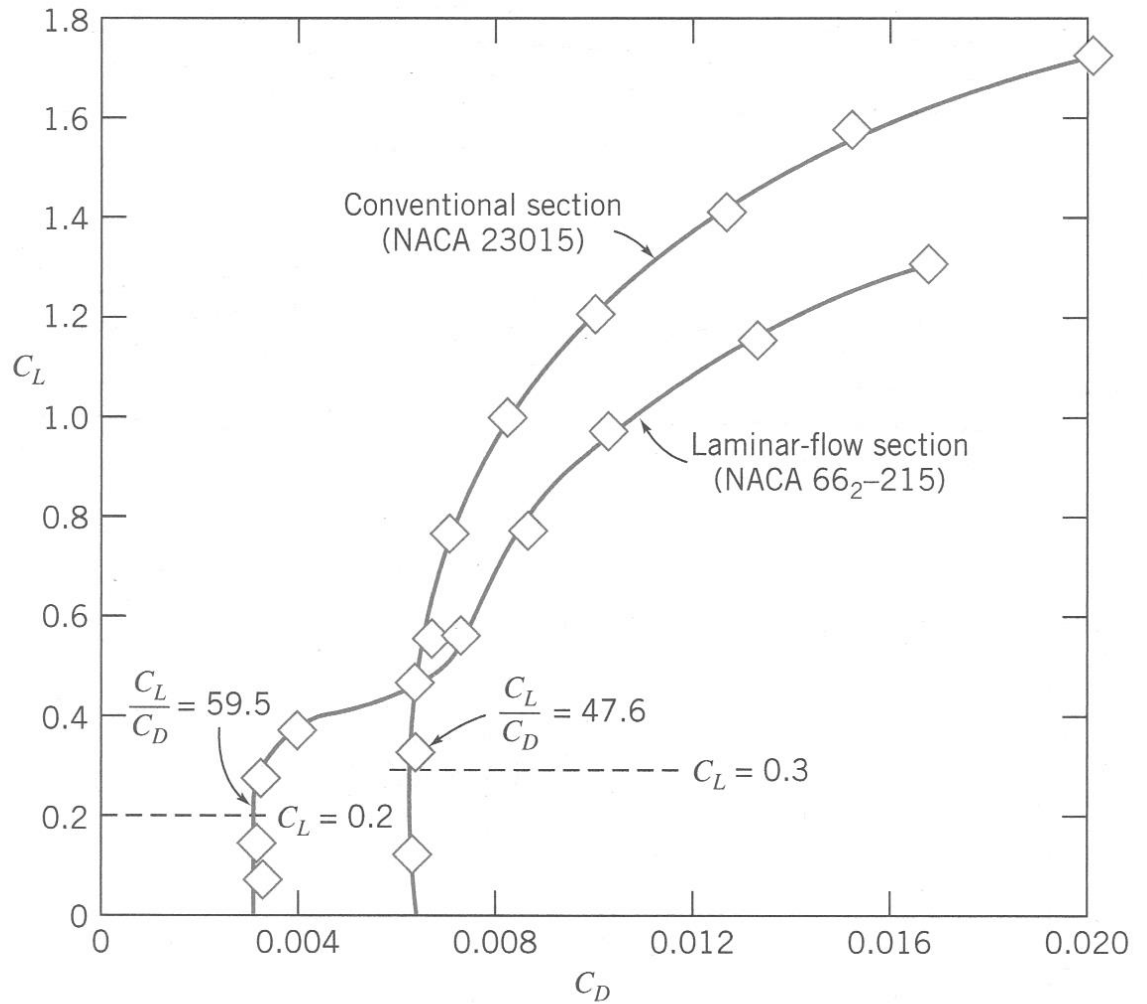


(a) Lift coefficient vs. angle of attack

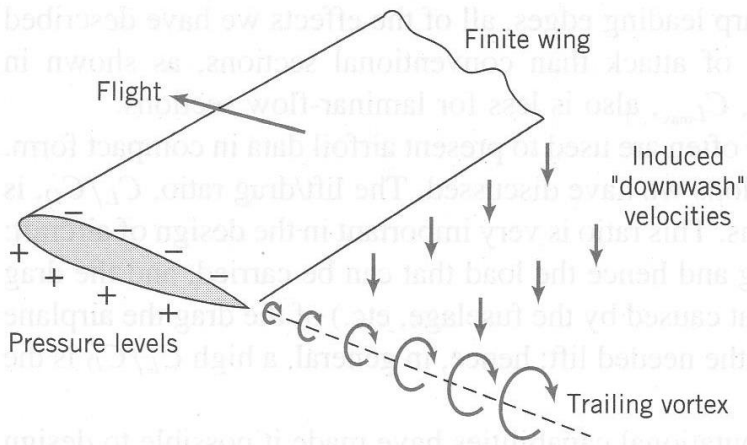


(b) Drag coefficient vs. angle of attack

**Fig. 9.17** Lift and drag coefficients versus angle of attack for two airfoil sections of 15 percent thickness ratio at  $Re_c = 9 \times 10^6$ . (Data from Abbott and von Doenhoff [21].)



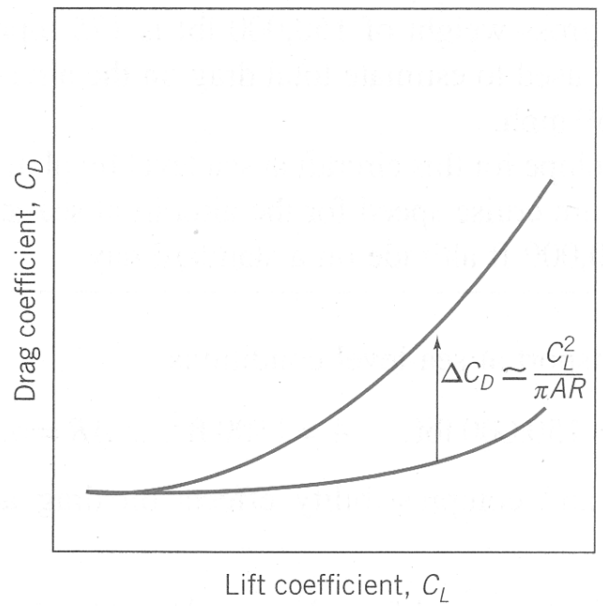
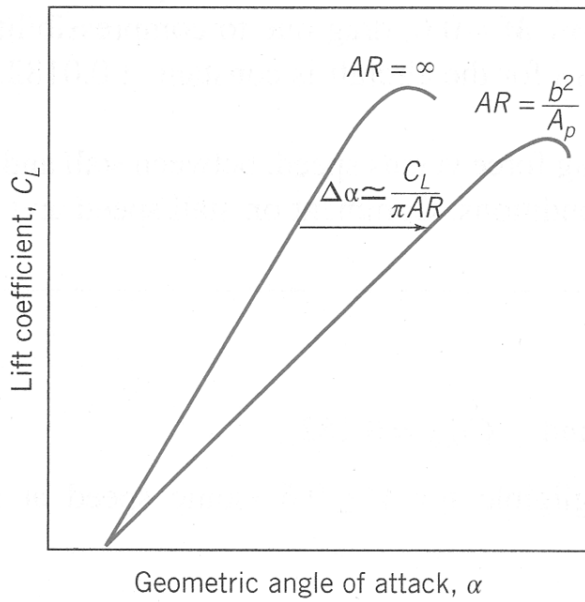
**Fig. 9.19** Lift-drag polars for two airfoil sections of 15 percent thickness ratio. (Data from Abbott and



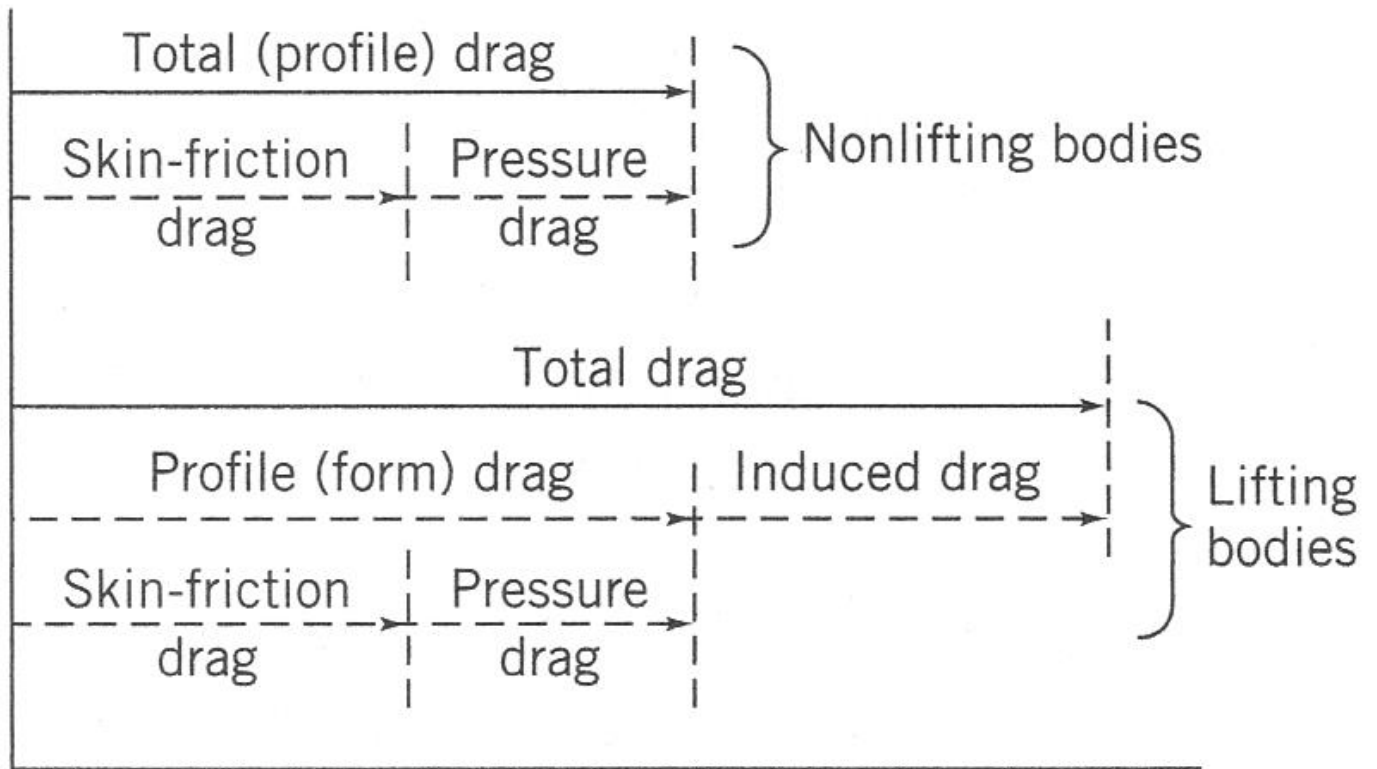
**Fig. 9.20** Schematic representation of the trailing vortex system of a finite wing.







**Fig. 9.21** Effect of finite aspect ratio on lift and drag coefficients for a wing.



**Fig. 9.22** Drag breakdown on nonlifting and lifting bodies.